Challenge Journal of STRUCTURAL MECHANICS

Vol.5 No.2 (2019)

Mindlin's theory buckling building codes dynamic analysis dynamic response earthquake elastic foundation finite element analysis finite element method nonlinear analysis operational modal analysis optimization prestressing pushover analysis reinforced concrete seismic analysis seismic design seismic isolation soil-structure interaction temperature effects thick plate wind

ISSN 2149-8024

TULPAR ACADEMIC PUBLISHING

Challenge Journal of Structural Mechanics

E-mail: *cjsmec@challengejournal.com*

Web page: *cjsmec.challengejournal.com*

TULPAR Academic Publishing
www.tulparpublishing.com

Challenge Journal of Structural Mechanics

CONTENTS

Research Articles

TULPAR ACADEMIC PUBLISHING

Challenge Journal of Structural Mechanics

Research Article

Effect of basalt, polypropylene and macro-synthetic fibres on workability and mechanical properties of self-compacting concrete

Zinnur Çelik [a,*], Ahmet Ferhat Bingöl [b]

[a] *Department of Civil Engineering, Pasinler Vocational School, Atatürk University, 25300 Erzurum, Turkey*
[b] *Department of Civil Engineering, Atatürk University, 25240 Erzurum, Turkey*

ABSTRACT

In this study, the effects of different fibre types on the workability and mechanical properties of self-compacting concrete were investigated. Fresh and hardened properties of self-compacting concrete, different fibre content 0.90, 1.35 and 1.80 kg/m^3 were evaluated using basalt, polypropylene and macro synthetic fibres with different fibre lengths of 24, 19 and 40 mm, respectively. The properties of fresh concrete were evaluated in terms of slump flowing, viscosity and flowability. In addition, compressive, flexural and splitting tensile strength were obtained from hardened concrete properties. To characterize mechanical properties 90 specimens were experimentally tested. The results show that the use of fibre reduces the workability of self-compacting concrete. On the other hand, tensile and flexural strength of the self-compacting fibre reinforced concrete increased with increasing fibre content, but it was determined that the fibre addition had no significant effect on the compressive strength.

ARTICLE INFO

Article history:
Received 3 February 2019
Revised 4 March 2019
Accepted 13 March 2019

Keywords:
Self-compacting concrete
Basalt fibre
Polypropylene fibre
Macro-synthetic fibre
Workability
Mechanical properties

1. Introduction

Self-compacting concrete (SCC) is a type of concrete that can be processed under its own weight without the need for vibration (Sahmaran et al., 2006; Uysal and Yılmaz, 2011; Bingol and Tohumcu, 2013). High range water- reducing superplasticizer chemical additives, powder material and/or viscosity regulators are used in the production of SCC. The main fresh concrete properties of SCC can be specified as filling ability, passing ability and segregation resistance (Liu, 2010; El-Dieb and Taha, 2012). Since its development in Japan in the mid-1980s, research has been conducted on SCC.

Fibre reinforced concrete is a composite material based on cement based matrix using short or long fibres. The use of fibre-reinforced concrete has recently increased due to the significant improvement of the properties of the fibres such as flexural strength, tensile strength, impact resistance and toughness of the concrete. It is also known that adding fibre to the concrete has little or no effect on the compressive strength and the modulus of elasticity (ACI Committee 544, 1988; Mazaheripour, 2011). The mechanical properties of fibre reinforced concrete are dependent on many factors including the aspect ratio (fibre length / equivalent diameter) of the fibres, volume percentage, physical and mechanical properties of the fibres (CNR-DT 204, 2007; Smarzewski, 2019). The addition of fibre in SCC improves the mechanical properties of hardened concrete, but also has a negative effect on the fresh properties of the SCC, such as the slump flow diameter, passing and filling ability. The most commonly used fibre types are steel, polypropylene, glass, carbon, basalt, aramid and polyethylene.

In the study conducted by Jiang et al. (2014), the behaviour of concrete produced with basalt fibre was investigated using the fibre amounts ranging from 0.05% to 0.3%. It was stated that the addition of fibre into concrete increases the compressive strength by 3.66% to 2.62%, respectively. The effect of the addition of basalt fibre on the mechanical properties of concrete was investigated by Arslan (2016). The compressive strength of normal concrete tend to increase by an average of 7.25% in the presence of 3 kg/m^3 content of basalt fibre.

* *Corresponding author*. Tel.: +90-442-661-3982 ; Fax: +90-442-661-3713 ; E-mail address: zinnur.celik@atauni.edu.tr (Z. Çelik)
ISSN: 2149-8024 / DOI: https://doi.org/10.20528/cjsmec.2019.02.001

Dias and Thaumaturgo (2005) reported that the addition of basalt fibre at 0.5% volume fraction caused a 3.9% reduction on the compressive strength at 28 days. For polypropylene FRC, some studies (Mazaheripour et al., 2011; Komlos et al., 1995), reported that polypropylene fibres have no significant effect on the compressive strength of concrete.

Algin and Ozen (2018) investigated influence of basalt fibre on splitting tensile and flexural strength of SCC. It was stated that the addition of basalt fibre into SCC increases the splitting tensile and flexural strength by 15% and 19%, respectively. Jiang et al. (2014) reports that the incorporation of basalt and polypropylene fibres at a rate of 0.05–0.3% induces the increase in the flexural strength by the ranges of 6.30% to 9.58% and 3.94% to 6.96%. Branston et al. (2016) stated that the flexural strength of the 36 mm diameters of 4, 8 and 12 kg/m^3 basalt fibre reinforced concrete improved by 8.40%, 16.05% and 21.72%, respectively. The effect of basalt fibre on high strength concrete was investigated by Zhang et al. (2018), it was stated that the highest flexural strength value is obtained in the case of using 0.1% by volume of fibre, and there is no significant change in strength in 0.2% and 0.3%.

2. Experimental Program

2.1. Materials

In this study, two different aggregates were used as aggregate size: fine aggregate (0-5 mm) and coarse aggregate (5-12). The specific gravity of the fine and coarse aggregate was 2.62 and 2.67 g/cm^3, respectively. CEM 1 42.5 R Portland cement was used to obtain concrete mixtures. To provide the workability properties of the self-compacting concrete, the cement was replaced with fly ash by 20% of its weight. The chemical, physical and mechanical properties of cement and fly ash used in concrete mixtures are shown in Table 1.

Table 1. Properties of cement and fly ash.

Chemical composition	CEM 1 42.5 R	Fly ash
SiO_2 (%)	18.10	60.61
Al_2O_3 (%)	4.48	20.81
Fe_2O_3 (%)	3.09	7.36
CaO (%)	63.65	2.44
MgO (%)	2.58	1.64
SO_3 (%)	2.84	0.51
Na_2O (%)	3.90	0.56
K_2O (%)	0.21	1.91
CI (%)	0.015	0.0067
Loss on ignition (%)	3.90	2.71
Insoluble Residue (%)	0.55	89.19
Physical and mechanical characteristics	**CEM 1 42.5 R**	**Fly ash**
Specific gravity (g/cm^3)	3.12	2.33
Specific surface (cm^2/g)	3698	2475
Compressive strength (MPa)		
2nd day	27.90	
28th day	58.00	

Detailed properties provided by manufacturer and basalt, macro-synthetic and polypropylene fibres are presented in Table 2 and Fig. 1. In addition, high range water reducing admixture was used by weight of cement for concrete mixtures in order to obtain self-compactability concretes.

Table 2. Properties of fibres.

Fibre type	Length (mm)	Diameter (μm)	Modulus of elastisity (GPa)	Tensile strength (MPa)	Density (g/cm^3)
Basalt	24	13-20	88	4000-4500	2.80
Polypropylene	19	18-20	3.0-3.5	350	0.91
Macro-synthetic	40	440	9.5	620	0.92

Fig. 1. Polypropylene, basalt and macro-synthetic fibre.

2.2. Concrete mix design

In this study, the ratio of coarse aggregate and fine aggregate content (50–50% of total aggregate by volume). The W/B ratio was kept constant at 0.42. The mixture design included 2% superplasticizer by weight of total cement. Table 3 shows the details of mix proportions of ten different concrete mixtures prepared in this research.

2.3. Testing methods

To determine the flow properties of self-compacting concrete, slump flow test, V-funnel and L-box test was performed instantly after mixing the concrete. The workability tests were conducted before casting according to the EFNARC suggestions. According to EFNARC, SCC classes and conformity criteria are presented in Table 4.

Table 3. Concrete mixture proportions.

Concrete	Cement (kg/m^3)	Fly ash (kg/m^3)	W/B	Coarse aggregate (5-12 mm.) (kg/m^3)	Fine aggregate (0-5 mm.) (kg/m^3)	Superplasticizer (%)	Fibre (kg/m^3)
Control	425	75	0,42	816	802	2	------
BF 0.90	425	75	0,42	816	802	2	0,90
BF 1.35	425	75	0,42	816	802	2	1,35
BF 1.80	425	75	0,42	816	802	2	1,80
PPF 0.90	425	75	0,42	816	802	2	0,90
PPF 1.35	425	75	0,42	816	802	2	1,35
PPF 1.80	425	75	0,42	816	802	2	1,80
MSF 0.90	425	75	0,42	816	802	2	0,90
MSF 1.35	425	75	0,42	816	802	2	1,35
MSF 1.80	425	75	0,42	816	802	2	1,80

Table 4. Conformity criteria for the properties of SCC.

Slump-Flow classes	Slump flow in mm
SF1	550 to 650
SF2	660 to 750
SF3	760 to 850
Viscosity classes	V-funnel time in s
VF1	≤ 8
VF2	9 - 25
Passing ability classes (L-box)	Passing ability
PA1	≥ 0,80 with 2 rebars
PA2	≥ 0,80 with 3 rebars

The compressive strength of the self-compacting concrete batches was obtained by three 150x150x150 mm cube samples according to ASTM C39. Splitting tensile testing was completed following the guidelines of ASTM C496. The splitting tensile strength was determined on the cylindrical samples measuring 100 mm diameter and 200 mm height. The flexural strength was completed according to ASTM C78. Concrete prisms 400 mm in length and 100 mm by 100 mm in cross-section were subjected to third point loading using a compression testing machine with a 3000 kN capacity. The compressive, splitting tensile and flexural strength is computed by averaging the results from three samples.

3. Results and Discussion

3.1. Workability properties

In order to determine the workability properties of fresh self-compacting concrete samples, slump flow test, L-box test and V-funnel test were carried out on the samples and the results are presented in Table 5.

As a result of the investigation of the fresh concrete properties of the SCC, it is seen that the use of fibre negatively effects the workability properties of fresh concrete. The flow spread for all groups of concrete mixes that was measured to be in between 570 and 720 mm. The test results demonstrated that control, BF 0.90, BF 1.35 and MSF 0.90 group falls in SF2 class which is suitable for many normal applications (e.g. walls, columns). Use of fibre decreased workability of the fresh concrete and BF 1.80, MSF 1.35, MSF 1.80 and all polypropylene fibre groups determined to be in SF1 class which is appropriate for unreinforced or slightly reinforced concrete structures that are cast from the top with free displacement from the delivery point, casting by a pump injection system or sections that are small enough to prevent long horizontal flow.

When the V-funnel flow times of the mixture samples are evaluated, the control, BF 0.90 and BF 1.35 series falls in VF-1 class specified in the standard and the other mixture samples are in the VF-2 class. The slump flow diameter and the V-Funnel flow time of the mixtures are shown in Fig.2. According to EFNARC, passing ability describes the capacity of the fresh mix to flow through confined spaces and narrow openings such as areas of congested reinforcement without segregation, loss of uniformity or causing blocking. The L-box tests are used to evaluate the passing ability of SCC. According to the results of the L-box test, were obtained the results below the target value of 0.80. Control, BF 0.90, BF 1.35, PPF 0.90 and MSF 0.90 group falls in PA1 class which has good filling ability even with congested reinforcement, capable of self-levelling and generally has the best surface finish.

Table 5. Concrete mixture proportions.

Concrete	Slump-flow diameter (mm)	V funnel time (s)	L- box blocking ratio (H_2/H_1)
Control	720	5,50	0,88
BF 0.90	680	7,03	0,85
BF 1.35	650	7,30	0,81
BF 1.80	630	8,16	0,76
PPF 0.90	640	8,10	0,83
PPF 1.35	600	8,80	0,79
PPF 1.80	570	9,73	0,74
MSF 0.90	660	10,30	0,82
MSF 1.35	630	10,90	0,76
MSF 1.80	590	11,50	0,71

3.2. Results of the mechanical test

3.2.1. Compressive strength

Compressive strength testing was performed at 28 days and the results are shown in Fig. 3 for all SCC series. In this study the compressive strength of polypropylene, basalt and macro-synthetic FRSCC shows no obvious improvement. Compared with the control concrete, the compressive strength of the samples reinforced with basalt fibre with the fibre content of 0.90, 1.35 and 1.80 kg/m3 increase by 2.43%, 3,58% and 4.20%, respectively. When adding PPF and MSF with the content of 0.90, 1.35 and 1.80 kg/m3, the compressive strength improvement of PPF reinforced concrete ranges from 1.90% to 3.63% and the compressive strength improvement of MSF reinforced concrete ranges from 0.73% to 1.97%. For the concrete mixtures containing the macro - synthetic fibre content of 1.80 kg/m3, the compressive strength is lower than the mixture containing the content of 0.90 kg/m3 and 1.35 kg/m3, but the results are higher than the control sample.

Basalt, macro-synthetic and polypropylene fibres, have a tendency to reduce the workability of fresh concrete and resulting in the risk of reduction in the concrete compressive strength. In addition, the fibres create void regions in FRSCC and failure may occur due to them. In this study, low fibre content had a positive effect on compressive strength. The increase in compressive strength of FRC reported by some experimental studies may have been the effect of the reduction in water/cement ratio for cement hydration, which resulted in a higher compressive strength of the hydrated cement paste and not by the beneficial fibres effect (Smarzewski, 2019).

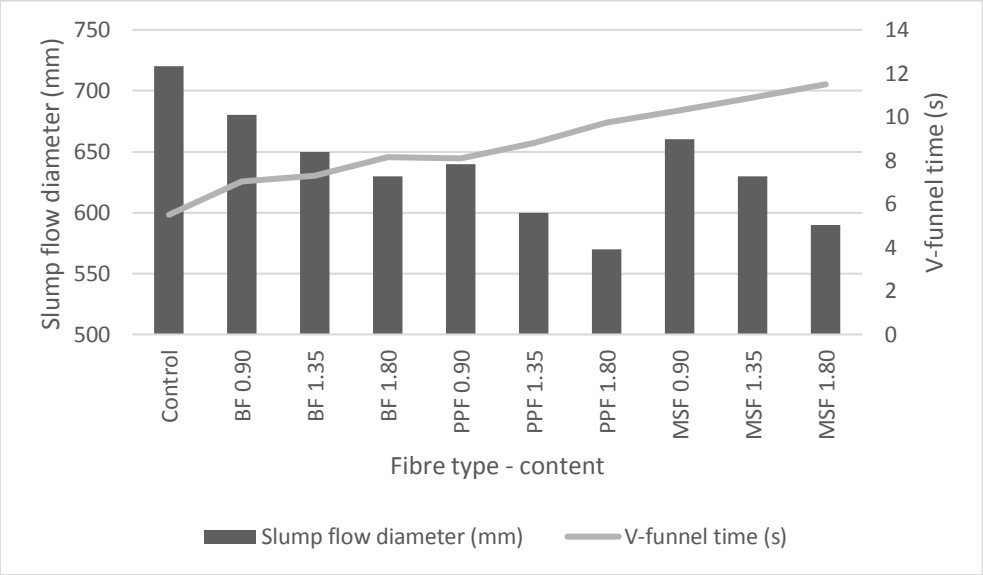

Fig. 2. Slump flow and V-funnel test results of FRSCC.

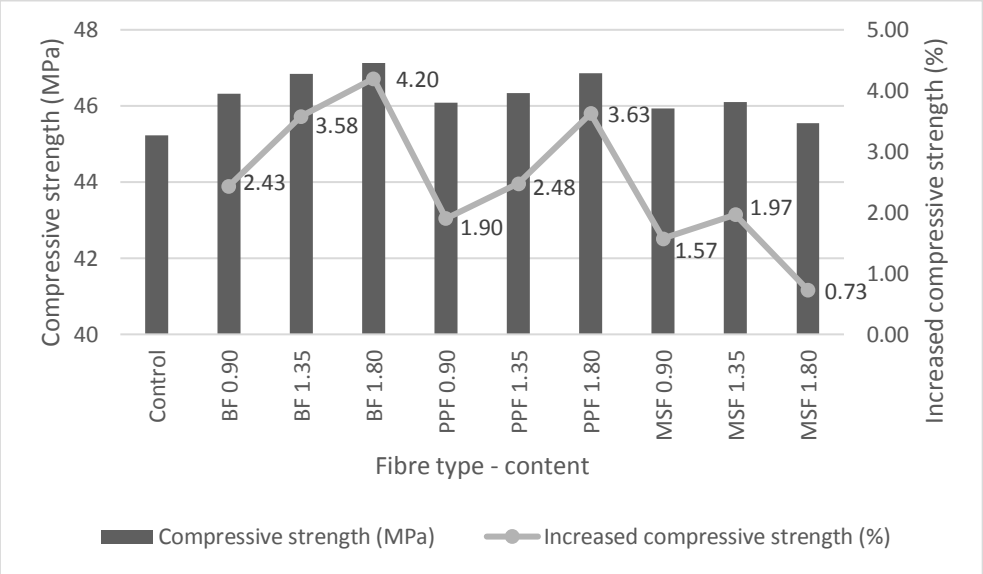

Fig. 3. Compressive strength test results of FRSCC.

3.2.2. Splitting tensile strength

The strength–effectiveness of the splitting tensile strength of the fibre concrete at 28 days shows Fig.4.

Compared with control concrete, the use of fibre significantly increased the splitting tensile strength of FRSCC and the highest splitting tensile strength was obtained in the MSF 1.80 series. The splitting tensile strength of the samples reinforced with macro synthetic fibre with the fibre content of 0.90, 1.35 and 1.80 kg/m^3 increase by 9.68%, 14.84% and 17.42% compared with the control concrete, respectively. Longer fibres show more obvious bridging effect and stronger pulling out resistance, which would contribute to strength development (Jiang et al., 2014). The splitting tensile strength improve of BF and PPF reinforced concrete ranges from 7.10% to 16.77% and 5.81% to 14.19% respectively at 28 days. Previous studies have stated that the adding fibre to concrete induced a significant increase on the splitting tensile strength. Jiang et al. (2014) reported that the splitting tensile strengths of the basalt and polypropylene fibre at 0.05% volume fraction, compared with control concrete were 6.30% and 3.94% higher, respectively. Arslan (2016) reported a 10.1% increase in the splitting tensile strength of concrete containing 2 kg/m^3 basalt fibre.

3.2.3. Flexural strength

Flexural strength testing was performed at 28 days and the results are shown in Fig. 5 for all SCC series. The maximum increase of flexural strength was recorded 8.61% in series BF 1.80 compared to the control concrete. Also, when added basalt fibres with fibre content of 0.90 kg/m^3 and 1.35 kg/m^3, the flexural strength increased 4.65% and 6.34%, respectively.

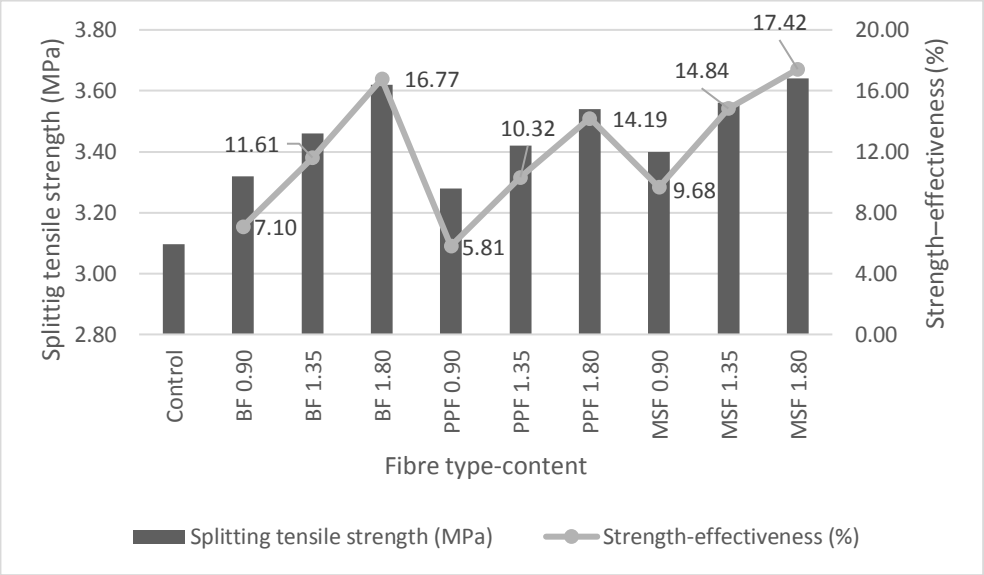

Fig. 4. Splitting tensile strength test results of FRSCC.

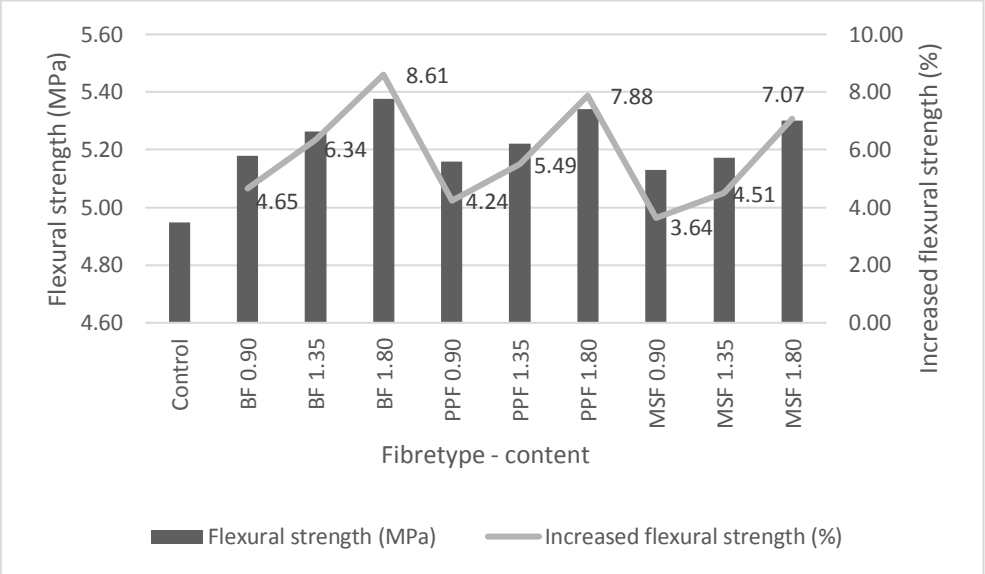

Fig. 5. Flexural strength test results of FRSCC.

The flexural strength results of PPF and MSF series with the fibre content of 0.90, 1.35 and 1.80 kg/m^3 cause the increase by ranges from 4.24% to 7.88% and 3.64% to %7.07%, compared to the control concrete. In the examination of the fracture patterns of the specimens during the flexural strength test, a more ductile behavior was observed in polypropylene and macro synthetic fibre mixtures, whereas the basalt fibre mixtures showed a more brittle behavior. Mazaheripour et al. (2011) stated that the flexural strength of the polypropylene reinforced concrete increased by 4.45% at a fibre content 1.82 kg/m^3. Effect of the content of basalt fibre on the flexural strength was investigated by Kabay (2014), 2 kg/m^3 content of basalt fibre increased the flexural strength of concrete 6.35%. Arslan (2016) reported that 2 kg/m^3 content of polypropylene fibre increased the flexural strength of the concrete 25.3%, compared with plain concrete. Mechanical properties values obtained from are given in Table 6.

4. Conclusions

In the study, workability and mechanical properties of FRSCC mixtures were determined. The results obtained in the scope of this study are indicated below.

As a result obtained indicate that addition of BF, PPF and MSF to the self-compacting concrete leads to significantly reduce in the workability of concrete. Compared with the control concrete, the slump flow diameter of the mixtures reinforced with BF, PPF and MSF with the fibre content of 1.80 kg/m^3 decrease by 12.50%, 20.83% and 18.05%, respectively. When the V funnel results are examined, the control, BF 0.90 and BF 1.35 series fall into the VF-1 class specified in the standard and the other mix samples are in the VF-2 class.

Although the use of fibre in SCC series has no significant effect on compressive strength, the highest compressive strength results were obtained in the BF series. Furthermore, during the compressive strength test, the

fibres restricted the lateral expansion of the concrete and delayed the fracture.

Compared with control group, the results of flexural strength of the SCC series, adding 0.90, 1.35 and 1.80 kg/m^3 basalt, polypropylene and macro synthetic fibre, the flexural strength increase of concrete ranges from 4.65% - 8.61%, 4.24% - 7.88% and 3.64% - 7.07%, respectively. The PF and MSF series showed a ductile post peak behavior, whereas the BF series brittle failure after reaching the peak load.

Adding BF, PPF and MSF notably increased splitting tensile strengths of FRSCC with according to control mixture. The highest splitting tensile strength values were obtained from MSF 1.80 specimens.

Table 6. Mechanical results of FRSCC.

Concrete	Compressive strength (MPa)	Splitting tensile strength (MPa)	Flexural strength (MPa)
Control	45.22	3.10	4.95
BF 0.90	46.32	3.32	5.18
BF 1.35	46.84	3.46	5.26
BF 1.80	47.12	3.62	5.38
PPF 0.90	46.08	3.28	5.16
PPF 1.35	46.34	3.42	5.22
PPF 1.80	46.86	3.54	5.34
MSF 0.90	45.93	3.40	5.13
MSF 1.35	46.11	3.56	5.17
MSF 1.80	45.55	3.64	5.30

References

ACI Committee 544 (1988). Measurements of properties of fibre reinforced concrete. *ACI Materials Journal*, 85(6), 583–593.

Algın Z, Ozen M (2018). The properties of chopped basalt fibre reinforced self-compacting concrete. *Construction and Building Materials*, 186, 678-685.

Arslan ME (2016). Effects of basalt and glass chopped fibres addition on fracture energy and mechanical properties of ordinary concrete: CMOD measurement. *Construction and Building Materials*, 114, 383-391.

ASTM C39 (1994). Standard test method for compressive strength of cylindrical concrete specimens, West Conshohocken, PA.

ASTM C496 (1994). Standard test method for split tensile strength of cylindrical concrete specimens, West Conshohocken, PA.

ASTM C78 (2016). Standard test method for flexural strength of concrete (using simple beam with third-point loading). *Annual Book of ASTM Standards*. American Society for Testing and Materials, West Conshohocken, PA.

Bingol AF, Tohumcu I (2013). Effects of different curing regimes on the compressive strength properties of self-compacting concrete incorporating fly ash and silica fume. *Materials and Design*, 51, 12-18.

Branston J, Das S, Kenno SY, Taylor C (2016). Mechanical behaviour of basalt fibre reinforced concrete. *Construction and Building Materials*, 124, 878-886.

CNR-DT 204 (2006, 2007). Guide for the design and construction of fibre-reinforced concrete structure. *CNR*.

Dias DP, Thaumaturgo C (2005). Fracture toughness of geopolymeric concretes reinforced with basalt fibres. *Cement and Concrete Composites*, 27(1), 49-54.

EFNARC (2005). The European Guidelines for Self Compacting Concrete-Specification, Production and use, *The European Federation of Specialist Construction Chemicals and Concrete Systems*.

El-Dieb AS, Taha MMR (2012). Flow characteristics and acceptance criteria of fibre-reinforced self-compacted concrete (FR–SCC). *Construction and Building Materials*, 27, 585-596.

Jiang C, Fan K, Wu F, Chen D (2014). Experimental study on the mechanical properties and microstructure of chopped basalt fibre reinforced concrete. *Materials and Design*, 58, 187-193.

Kabay N (2014). Abrasion resistance and fracture energy of concretes with basalt fibre. *Construction and Building Materials*, 50, 95-101.

Komlos K, Babal B, Nurnbergerova T (1995). Hybrid fibre reinforced concrete under repeated loading. *Nuclear Engineering Design*, 156, 195–200.

Liu M (2010). Self-compacting concrete with different levels of pulverized fuel ash. *Construction and Building Materials*, 24, 1245-1252.

Mazaheripour H, Ghanbarpour S, Mirmoradi SH, Hosseinpour I (2011). The effect of polypropylene fibres on the properties of fresh and hardened lightweight self-compacting concrete. *Construction and Building Materials*, 25, 351-358.

Sahmaran M, Christianto HA, Yaman İO (2006). The effect of chemical admixtures and mineral additives on the properties of self-compacting mortars. *Cement and Concrete Composites*, 28, 432-440.

Smarzewski P (2019). Influence of basalt-polypropylene fibres on fracture properties of high performance concrete. *Composite Structures*, 209, 23-33.

Uysal M, Yılmaz K (2011). Effect of mineral admixtures on properties of self-compacting concrete. *Cement and Concrete Composites*, 33, 771-776.

Zhang J, Zhao Y, Li H (2018). Effect of basalt fibres on mechanical properties of high-performance concrete containing supplementary cementitious materials. *RILEM Bookseries*, 15, 181-187.

Challenge Journal of Structural Mechanics

Research Article

A comparative study of concrete strength prediction using artificial neural network, multigene programming and model tree

Preeti Kulkarni *, Shreenivas N. Londhe, Pradnya R. Dixit

Department of Civil Engineering, Vishwakarma Institute of Information Technology, Pune 411048, India

ABSTRACT

In the current study 28 day strength of Recycled Aggregate Concrete (RAC) and Fly ash (class F) based concrete is predicted using Artificial Neural Network (ANN), Multigene Genetic Programming (MGGP) and Model Tree (MT). Four sets of models were designed for per cubic proportions of materials, Properties of materials and non-dimensional parameters as input parameters. The study shows that the predicted 28 day strength is in good agreement with the observed data and also generalize well to untrained data. ANN outperforms MGGP and MT in terms of model performance. Output of the developed models can be presented in terms of trained weights and biases in ANN, equations in MGGP and in the form of series of equations in MT. ANN, MGGP and MT can grasp the influence of input parameters which can be seen through Hinton diagrams in ANN, input frequency distribution in MGGP and coefficients of input parameters in MT. The study shows that these data driven techniques can be used for developing model/s to predict strength of concrete with an acceptable performance.

ARTICLE INFO

Article history:
Received 23 February 2019
Revised 26 April 2019
Accepted 15 May 2019

Keywords:
Recycled aggregate concrete
Fly ash concrete
Artificial neural network
Multigene genetic programming
Model tree

1. Introduction

Recycled Aggregates and fly ash are the alternative materials used in concrete which can be termed as a step towards use of waste materials in concrete. Ascertaining strength of such concrete is a tedious and difficult task owing to the different properties of Recycled aggregates and fly ash (Hansen and Narud, 1983; Yueh and Hwang, 2006; Ryu, 2002). Determination of compressive strength of concrete has great importance as it offers an option to do the essential modification on the mix proportion to avoid circumstances where concrete does not attain the design strength and also for more economic use of raw material and fewer construction failures, thus reducing construction cost. Traditional determination of compressive strength of concrete needs actual testing which requires time and materials, which can be reduced by using data driven techniques like Artificial Neural Network (ANN), Genetic Programming (GP), and Model Tree (MT) etc. Prediction of compressive strength of concrete has been an active area of research in last two decades or so (Dias and Pooliyadda, 2001; I-Cheng, 2007; Ni and Wang, 2000; Ahmet et al., 2006; Adriana et al., 2013; Duan et al., 2013; Deshpande et al., 2014; Gorphade et al., 2014; Sarıdemir, 2010; Bayazidi et al., 2014). Relatively new techniques of GP and MT have been used sparingly for modeling the compressive strength of concrete. ANN models were developed to predict the strength and slump of ready mix concrete with admixtures in which the input parameters were non-dimensional ratios transformed from the material weights per unit volume. Neural network was also developed with the natural logarithms of both inputs and outputs (Dias and Pooliyadda, 2001). Weights of mixes per unit volume were considered as input parameters to predict slump of High Performance Concrete (HPC) using ANN (I-Cheng, 2007). A Three layered neural network model was built to implement the complex nonlinear relationship between the inputs (11 factors that influence concrete strength) and the output (concrete strength). The neural network models give high prediction accuracy, and the research results conform to some rules of mix proportion of concrete (Ni and Wang, 2000). ANN models were developed to predict the Compressive

* *Corresponding author*. Tel.: +91-955-252-5907 ; E-mail address: preeti.kulkarni@viit.ac.in (P. Kulkarni)
ISSN: 2149-8024 / DOI: https://doi.org/10.20528/cjsmec.2019.02.002

Strength and slump of High Strength Concrete (HSC) with input parameters such as water to binder ratio, water content, fine aggregate ratio, fly ash content etc. (Ahmet et al., 2006). ANN is used as an attempt to obtain more accurate concrete strength prediction based on parameters like concrete mix design, size and shape of specimen, curing technique and period, environmental conditions, etc. (Gupta et al., 2006). ANN with mix proportions as input parameters was used to predict strength of concrete from ready-mixed concrete companies (Jong-In Kim et al., 2004). Particularly in the field of RAC, ANN was used to predict strength of RAC (Adriana et al., 2013; Duan et al., 2013; Deshpande et al., 2014). Application of Genetic Algorithm based neural network models for predicting the Compaction factor, VB time and Compressive strength, Tensile strength, Flexural strength and Young's modulus of High performance concrete showed a prediction accuracy of 95% (Gorphade et al., 2014). In a study, two models using gene expression programming (GEP) approach were developed for predicting compressive strength of concrete containing rice husk ash at the age of 1, 3, 7, 14, 28, 56 and 90 days (Sarıdemir, 2010). MGGP as a technique was utilized to predict modulus of elasticity of concrete. A general model proposed for Normal strength concrete and High strength concrete using the 28 day strength data (Bayazidi et al., 2014). Model Tree (MT) was used to predict strength of conventional and Recycled aggregate concrete (Deshpande et al., 2014; Deepa et al., 2010).

The study concluded that ANN facilitates a better correlation among inputs and output and displays a good performance. Very few applications of GP (specifically MGGP) have been reported in recent literature focused on predicting strength of concrete. Similarly very few works can be seen which used MT to predict the concrete strength (CS). The study mentioned earlier focused mainly on performance of tool used rather than discussing the influence of input parameters on output which is necessary, for the tag of 'Black box' on these techniques to be removed. In the present work, three techniques viz. Artificial Neural Network (ANN), MultiGene Genetic Programming (MGGP) and Model Tree (MT) are used separately to develop models to predict strength of Recycled aggregate concrete and Fly ash based concrete respectively. Secondly, in total 8 models for each technique were developed with Mix proportions of materials, properties of materials and non-dimensional parameters as input parameters for developing different models. The data sets were designed in the said way so that the study is not limited to only type of input parameter/s for a similar output. Third, the influence of parameters affecting the strength of concrete are shown in the form of Hinton diagram in ANN, in the form of coefficients and input frequency in MGGP and coefficients of parameters in MT. Fourth, the comparative analysis of the modeling approaches (ANN, MGGP and MT) are validated with the observed values and best approach is suggested for predicting the 28 day compressive strength of concrete.

The paper is further organized as follows: The next section gives an overview of ANN, GP-MGGP and MT techniques. The information about data used is provided in following section followed by the methodology adopted. The results of models developed and influences of parameters are discussed in the next section followed by concluding remarks.

2. Modeling Techniques

In the current study, prediction of 28 day concrete strength (CS) for RAC and Fly ash based concrete is done using Artificial Neural Networks, Genetic Programming-Multi Gene Genetic Programming, and Model Tree with M5 algorithm. These approaches are described in brief below.

2.1. Artificial Neural Network (ANN)

ANN is a soft computing technique involving an input layer, one or more hidden layer (s) and an output layer. The hidden layer is connected to the other layers by weights, biases and transfer functions. An error function is determined by the difference between network output and the target. The error is propagated back and the weight and biases are adjusted using some optimization technique which minimizes the error. The entire process called training is repeated for number of epochs (iterations) till the desired accuracy in output is achieved. Once the network is trained it can be used to validate against unseen data using trained weights and biases (The ASCE Task Committee, 2000; Maier and Dandy, 2000).

2.2. Genetic Programming (GP)

Genetic programming (GP) is a biologically inspired machine learning method that evolves computer programs to perform a task (usually represented by tree structures) and then breeding together the best performing trees to create a new population. The three genetic operations are as follows: Reproduction, Cross over and Mutation (Londhe and Dixit, 2012). In MGGP, multigene individual consists of one or more genes, each of which is a "traditional" GP tree (Searson et al., 2010). Genes are acquired incrementally by individuals in order to improve fitness (e.g. to reduce a model's sum of squared errors on a data set). The overall model is a weighted linear combination of each gene. The resulting pseudo-linear model can capture non-linear behavior. When the transformations are forced to be low order (by restricting the GP tree depth), allows the evolution of accurate, relatively compact mathematical models of predictor – response (input – output) data sets, even when there are a large number of input variables. For example, the multigene model shown in Fig. 1 predicts an output variable using input variables x1, x2 and x3.

This model structure contains non-linear terms (e.g. the hyperbolic tangent) but is linear in the parameters with respect to the coefficients d0, d1 & d2. In practice, the user specifies the maximum number of genes Gmax a model is allowed to have and the maximum tree depth Dmax any gene may have and therefore can exert control over the maximum complexity of the evolved models. In particular, we have found that enforcing stringent tree depth restrictions (i.e. maximum depths of 4 or 5 nodes)

often allows the evolution of relatively compact models that are linear combinations of low order non-linear transformations of the input variables. Multigene GP combines the power of classical linear regression with the ability to capture non-linear behavior without needing to pre-specify the structure of the non-linear model (Searson et al., 2010; Searson et al., 2007). The uniqueness of the multi-gene genetic programming based model is that it automatically evolves a mathematical expression in a symbolic form which can be analyzed further to find which variables impact the final prediction and in what fashion (Pandey et al., 2015).

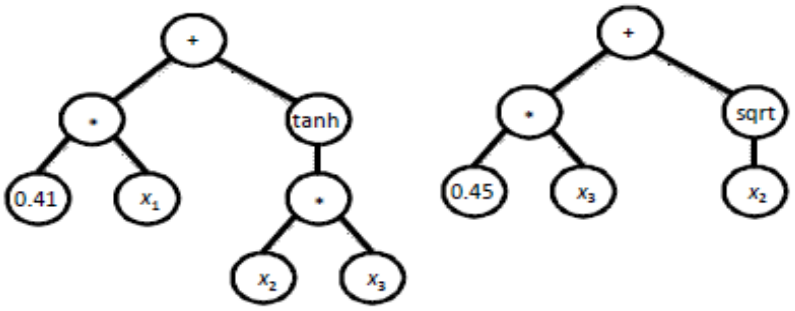

$$y = d_0 + d_1(0.41x_1 + \tanh(x_2x_3) + d_2(0.45x_3 + \text{sqrt}(x_2))$$

Fig. 1. Example of a Multigene symbolic model.

2.3. Model Tree (MT)

MT utilizes divide-and-conquer approach and provides rules for reaching the models at the leaf nodes. The linear models are then used to quantify the contribution of each attribute to the overall predicted value. M5P, a reconstruction of Quinlan's M5 algorithm is used for inducing trees of regression models and combines a conventional decision tree with the possibility of linear regression functions at the nodes. First, a decision-tree induction algorithm is used to build a tree and a splitting criterion is then used that minimizes the intra-subset variation in the class values down each branch. The splitting procedure in M5 stops if the class values of all instances that reach a node vary very slightly, or only a few instances remain. Second, the tree is pruned back from each leaf. When pruning an inner node is turned into a leaf with a regression plane. In comparison with classical regression trees, Model Trees deliver better compactness and prediction accuracy (Deepa et al., 2010; Quinlan, 1992).

3. Data and Model Development

For predicting concrete strength using ANN, MGGP and MT, experimentation work was carried out by the authors and few data was also collected from literature (Hansen and Narud, 1983; Yueh and Hwang, 2006; Ryu, 2002; Khatib, 2005; Padmini et al., 2003; Dapena et al., 2011; Corinaldesi, 2010; Fathifazl et al., 2009; Yong and Teo, 2009; Yaprak et al., 2011; ChakradharaRao et al., 2010; Schoppe, 2011; Kumutha and Vijai, 2010; Evangelista and Brito, 2010; Zega and Maio, 2003; Kou, 2006; Konin and Kouadio, 2011; Poon et al., 2004; Kotrayothar, 2012; Adnan et al., 2011; Poon et al., 2007; Domingo-Cabo et al., 2009; Pereira et al., 2012; Pelufo et al., 2009; Agarwal et al., 2011; Evangelista and Brito, 2004; Goncalves et al., 2004; Nikoo et al., 2015). The data used in the current work is divided into four sets i.e Set 1, Set 2, Set 3 and Set 4 and 2 models each. Set 1 is designed with process parameters related to Recycled aggregate concrete (RAC), Set 2 with Fly ash based concrete, Set3 with non-dimensional parameters for RAC and Set 4 with non-dimensional parameters of Fly ash based concrete. The data sets were designee in the said way so that the study is not limited to only one type of input parameters and number of data sets for a similar output.

The process parameters that have been used as model input parameters for models in Set1 are: Content of materials in kg/m^3 for Cement (RC, kg/m^3), Natural fine aggregate (RNFA, kg/m^3), Natural coarse aggregate-20mm (RNCA-20, kg/m^3), Natural coarse aggregate-10mm (RNCA-10, kg/m^3), Recycled coarse aggregate-20mm (RCA-20, kg/m^3), Recycled coarse aggregate-10mm (RCA-10, kg/m^3), Admixture(RA, kg/m^3) and water (RW, kg/m^3). Water absorption of conventional coarse aggregates (WA-NA, %) and water absorption of Recycled aggregates (WA-RA, %) were used as additional input parameters in Set 1: model 2. The input parameters for models in Set 2 were: Cement (FC, kg/m^3), Fly ash – Class F (F, kg/m^3), Fine aggregate (FNFA, kg/m^3), Natural coarse aggregate-20mm-1 (FNCA-20, kg/m^3), Natural coarse aggregate-10mm (FNCA-10, kg/m^3), water (FW, kg/m^3), and Admixture (FA, kg/m^3). Specific gravity of FNFA (FSP-NFA), Specific gravity of NCA-20 (FSP-20) and Specific gravity of NCA-10 (FSP-10) were additional input parameters in Set 2: model1. The input parameters for Set 3 were dimensionless parameters such as ratio of Water to cement ratio (RW/C), natural fine aggregate to total aggregate ratio (RNFA/A), Natural coarse aggregate-20mm to cement content (RNC20/A), Natural coarse aggregate-10mm to cement content (RNC10/A), Recycled coarse aggregate-20mm (RCA-20) to cement (RC20/C), Recycled coarse aggregate-10mm (RCA-10) to cement (RC10/C), water to total materials (RW/T). Replacement ratio (R-RR) was used as an additional parameter in Set 3:model2. The input parameters for Set 4

were non-dimensional parameters for Fly Ash based concrete namely Water to binder ratio (FW/B), machine made sand by aggregate ratio (FNFA/A), Natural coarse aggregate-20mm to cement ratio (FNCA20/C), Natural coarse aggregate-10mm to cement ratio (FNCA10/C) and water to total materials ratio (FW/T). Replacement ratio (F-RR) was used as an additional input parameter in Set 4:model2.

The output for each model is 28 day compressive strength of respective type of concrete (CS). The details of data used in developing the models are shown in Tables 1-4. The detail of models developed in each set is shown in Table 5.

Three layered Feed Forward Back-Propagation ANN models were developed using MATLAB 2016, to predict the 28 day CS and trained till a very low performance error (mean squared error) was achieved. All the networks were trained using Levernberg-Marquardt algorithm with 'log-sigmoid 'transfer functions in between the first (input) and second (hidden) layer and 'linear' transfer function between the second and third layer (output). Trial and error method was utilized to determine the optimal number of hidden neurons. MGGP models were developed using GPTIPS-2. Readers are referred for features of GPTIPS (Searson et al., 2007; Searson et al., 2010). The RMSE function was adapted for error minimization during runs (Searson et al., 2007; Searson et al., 2010). The adopted function set to develop the GP model are as shown in table 6 for each model. The parameters were selected which yielded best performance of the models. These settings were based on experience with the predictive modeling of other data sets of similar size, and so they may not be optimal. A fairly large number of population and generations were tested to find models with minimum error. The programs run until the number of generations were reached as in Table 6.

Table 1. Details of data in Set 1.

Sr. No	Parameters	Values (min-max)	Correlation with Output
1	RC (kg/m^3)	235-645	0.477
2	RNFA (kg/m3)	217-1050	0.004
3	RNCA-20mm (kg/m^3)	0-1508.640	0.118
4	RNCA-10mm (kg/m^3)	0-553	0.281
5	RCA-20mm (kg/m^3)	0-1508.640	-0.3011
6	RCA-10mm (kg/m^3)	0-840	-0.0989
7	RW (kg/m^3)	120-271	0.0451
8	RA (kg/m^3)	0-41.600	-0.3186
9	WA-RA (%)	0-10.600	-0.109
10	WA-NA (%)	0-3.560	-0.207
11	S (N/mm^2)	10.319-100.500	

Table 2. Details of data in Set 2.

Sr. No	Parameters	Values (min-max)	Correlation with Output
1	FC (kg/m^3)	130-460	0.861
2	F (kg/m^3)	0-120	-0.247
3	FNFA-1 (kg/m^3)	398-1011	-0.421
4	FNCA-20mm (kg/m^3)	0-958	-0.163
5	FNCA-10mm (kg/m^3)	482-1242	0.039
6	FW (kg/m^3)	127-202	0.099
7	FA (kg/m^3)	0-5.520	0.519
8	FSP-NFA	2.700-2.980	0.199
9	FSP-20	0-3.050	-0.036
10	FSP-10	2.850-3.040	0.225
11	S (N/mm^2)	12-60.2	

Table 3. Details of data in Set 3.

Sr. No	Parameters	Values (min-max)	Correlation with Output
1	FW/B	0.315-0.980	-0.843
2	FNFA/A	0.200-0.489	-0.197
3	FNC20/C	1.175-5.393	-0.622
4	FNC10/C	0-4.354	-0.499
5	FW/T	0.051-0.0867	0.107
6	F-RR	0-48	-0.48
7	S (N/mm^2)	12-60.200	

Table 4. Details of data in Set 4.

Sr. No	Parameters	Values (min-max)	Correlation with Output
1	RWC	0.229-0.860	-0.584
2	RNFA/A	0.148-1.566	0.085
3	RNC20/C	0-4.726	0.029
4	RNC10/C	0-2.196	0.204
5	RC20/C	0-5.184	-0.359
6	RC10/C	0-2.333	-0.125
7	RW/T	0.054-0.139	-0.25
8	R-RR	0-100	-0.251
9	S (N/mm^2)	10.319-100.5	

Table 5. Model development.

Sr. No	Set No	Model No.	Input Parameters	No. of Data Sets
1	Set 1 (Recycled Aggregate Concrete)	1-1	RC, RNFA, RNC20, RNC10, RC20, RC-10,RA, RW	226
		1-2	RC, RNFA, RNC20, RNC10, RC20, RC-10, RA, RW, WA-RA, WA-NA	226
2	Set 2 (Fly Ash based Concrete)	2-1	FC, F, FNFA, FNC20, FNC10, FA, FW	113
		2-2	FC, F, FNFA, FNC20, FNC10, FA, FW, FSP-NFA, FSP-NC20, FSPNC10, FW,FA	113
3	Set 3 (Non-Dimensional Parameters for Recycled Aggregates)	3-1	RWC, RNFA/A, RNC20/C, RNC10/C, RC20/C, RC10/C, RW/T	226
		3-2	RWC, RNFA/A, RNC20/C, RNC10/C, RC20/C, RC10/C, RW/T, R-RR	226
4	Set 4 (Non Dimensional parameters related to Fly Ash based Concrete)	4-1	FW/B, FNFA/A, FNC20/C, FNC10/C, FW/T	113
		4-2	FW/B, FNFA/A, FNC20/C, FNC10/C, FW/T, F-RR	113

Table 6. Parameter settings for the MGGP.

GP Parameters	Parameter Settings
Population size	1000
Number of generation	200,500
Selection method	tournament
Tournament size	15
Crossover rate	0.84
Mutation rate	0.14
Termination criteria	500 generation or fitness value less than 0.00 whichever is earlier
Maximum number of genes	6,8
Maximum tree depth	4,5,6
Mathematical operations	+, -, x, /, sin, cos, exp, √, exp,{}

The maximum allowable number of genes in an individual and the maximum tree depth directly influence the size of the search space and the number of solutions explored within the search space (Searson et al., 2007; Searson et al., 2010; Pandey et al., 2015). The allowable number of genes and tree depth were, respectively, set to optimal values as tradeoffs between the running time and the complexity of the evolved solutions (Searson et al., 2007; Searson et al., 2010; Pandey et al., 2015). The best MGGP models were chosen on the basis of providing the best fitness value on the training and testing data as well as the simplicity of the models (Bayazidi et al., 2014). All these parameter combinations were tested and 2 replications for each were carried out. Multiple individual runs are suggested where the populations are automatically merged after the completion of the runs. This approach mitigates problems with the possible loss of model diversity over a run and with the GP algorithm getting stuck in local minima (Searson, 2015). The overall number of optimal individual runs equals to 12x8x2=192 (6 group of models for each generations 200 and 500. Each generation with genes 6 and 8 and further each generation and gene with tree depth 4, 5 and 6. Thus 12 group of models each for generations 200 and 500 and 2 replications for each models. The methodology is adopted for set 1 with 4 models and set 2 with 4 models).

For Model Tree as a technique, M5P algorithm implemented in software WEKA was used for calibrating the model (Frank et al., 2016; Deepa, 2010). To check the accuracies and robustness of the model, the dataset was divided for training and testing purposes. From the available data, 70% was selected to be used for training purposes and the remaining 30% was used for model validation. The performance of the model was assessed by statistical measures like correlation coefficient (*r*) (Eq. (1)), Root mean squared error (*RMSE*) (Eq. (2)), Average absolute error (*AARE*) (Eq. (3)), Mean absolute error (*MAE*) (Eq. (4)), and Nash-Sutcliffe Efficiency (*E*) (Eq. (5)) (David and Gregory, 1999; Jain et al., 2008; Londhe, 2008). Lower *RMSE* indicates good prediction, but this statistic is biased towards to high error values. Coefficient of correlation (*r*) measures the degree of association between the observed and predicted values and *r* closer to 1 indicates an almost perfect linear relationship between them. The value of zero for the coefficient of efficiency (*E*) indicates that the observed mean is as good a predictor as the model, while negative values indicate that the observed mean is a better predictor than the model. *E* is sensitive to outliers (David and Gregory, 1999). The degree to which *RMSE* exceeds *MAE* is an indicator of the extent to which outliers (or variance in the differences between the modeled and observed values) exist in the data (David and Gregory, 1999; Jain et al., 2008; Londhe, 2008).

$$r = \frac{\sum(S_{obs} - \bar{S}_{obs})(S_{cal} - \bar{S}_{cal})}{\sqrt{\sum(S_{obs} - \bar{S}_{obs})^2 (S_{cal} - \bar{S}_{cal})^2}} \quad (1)$$

$$RMSE = \sqrt{\sum_{i=1}^{n} (S_{obs} - \bar{S}_{cal})^2 / n} \quad (2)$$

$$AARE = \frac{1}{N} \sum \left| \frac{(S_{cal} - S_{obs})}{S_{obs}} \right| \times 100 \quad (3)$$

$$MAE = \frac{\sum_{i=1}^{N} |S_{cal} - \bar{S}_{cal}|}{N} \quad (4)$$

$$E = 1 - \frac{\sum(S_{cal} - S_{obs})^2}{\sum(S_{obs} - \bar{S}_{obs})^2} \quad (5)$$

where S_{obs}=observed strength; S_{cal}=strength calculated from a model; $\bar{S}_{obs}$=average observed strength; $\bar{S}_{cal}$=average calculated strength; *n*=total number of data points predicted and all the summations run from 1 to *N*.

The architecture of ANN models and no. of equations developed for each model by MT and the parameters not considered in the equation developed by MGGP is shown in Table 7.

4. Results and Discussion

4.1. Models developed using ANN

Performance of each of the models developed in testing using the ANN technique is shown in Table 8.

Table 7. Details of models developed.

Set. No	Model No.	ANN Architecture	No. of equation in MT	MGGP parameters not considered in the equation
1	1-1	8:25:01	2	NIL
	1-2	10:23:01	11	NIL
2	2-1	7:13:01	3	NIL
	2-2	10:08:01	5	SP-NC20
3	3-1	7:24:01	2	NIL
	3-2	8:25:01	2	RNC20/C
4	4-1	5:16:01	1	NIL
	4-2	6:10:01	1	NIL

Table 8. Performance of models developed using ANN.

Set. No	Model No.	*RMSE* (m/s)	*MAE* (m/s)	*E*	*AARE*	*r*
1	ANN 1-1	5.759	4.3375	0.87934	11.4091	0.9440
	ANN 1-2	7.8139	5.9043	0.78034	14.6269	0.8890
2	ANN 2-1	3.6983	2.5631	0.85917	8.3445	0.9388
	ANN 2-2	4.0241	2.7790	0.83327	8.7192	0.9293
3	ANN 3-1	6.5255	4.6132	0.84508	11.9555	0.9219
	ANN 3-2	6.2345	4.4092	0.85859	10.8077	0.9268
4	ANN 4-1	3.2909	2.4703	0.87941	7.7395	0.9438
	ANN 4-2	3.5056	2.7136	0.88577	10.1742	0.9452

Fig. 2 shows the scatter plot for ANN 1-1. Comparison between measured & predicted values for strength characteristics of RAC for whole test data in Fig. 2 demonstrates that there are few scatters away from the line of equality between measured and predicted values. As shown, the proposed model for compressive strength of RAC has a reasonable accuracy with less scatter and a high value of correlation coefficient (r=0.94). Fig. 3 shows the Hinton diagram which depicts the influence of various parameters on the compressive strength of concrete in ANN.

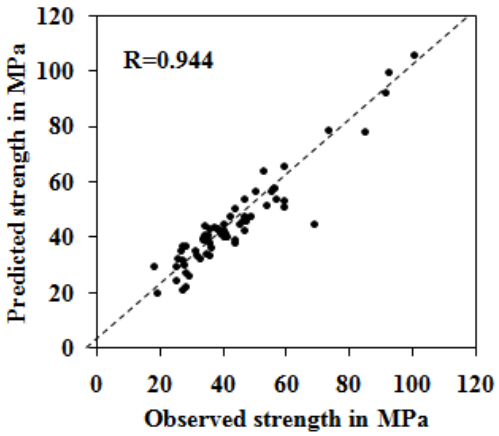

Fig. 2. Scatter plot for ANN1-1.

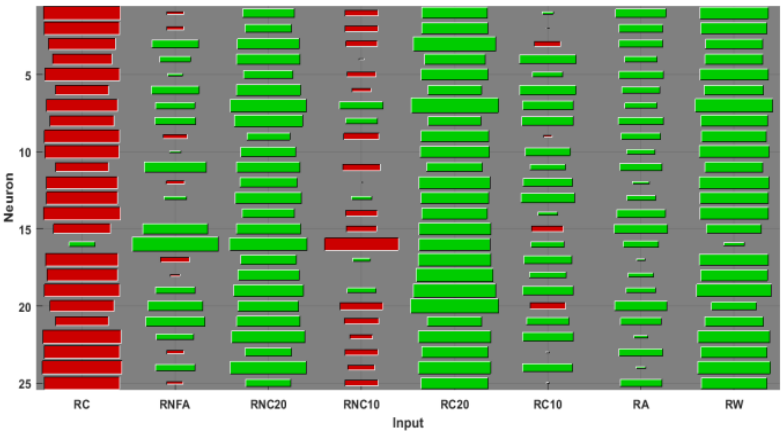

Fig. 3. Hinton diagram for ANN1-1.

A Hinton diagram is plot of weight matrix of a neural network, where the size of the square represents the magnitude, and the color represents the polarity (red=positive, green=negative). A Hinton diagram thus at a glance shows the units which are strongly active, which input parameters are off and which input parameters are intermediate in influence towards predicting the 28 day CS of RAC (Ahmet et al., 2006). A Hinton diagram for ANN1-1, shows maximum influence of cement content, water content followed by recycled aggregate

content in ANN1-1 on the CS of RAC. Hinton for ANN2-2 in Fig. 4 shows cement content, aggregate content and fly ash content as influential parameters in decreasing order followed by other input parameters. The Hinton diagram can thus eliminate the need for the sensitivity analysis. The scatter plot for ANN3-1 is shown in Fig. 5, shows over prediction of strength. Hinton diagram for ANN4-2 is as shown in Fig. 6 which shows aggregate to cement ratio and water to binder ratio as the highly influential parameters and with F-RR as the least influential parameter.

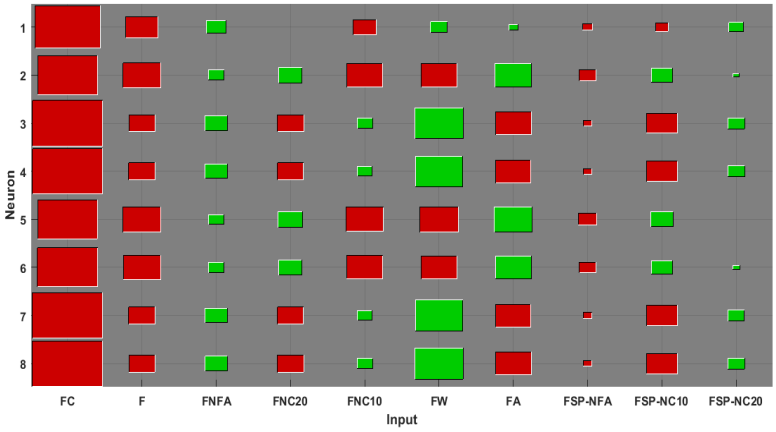

Fig. 4. Hinton diagram for ANN2-2.

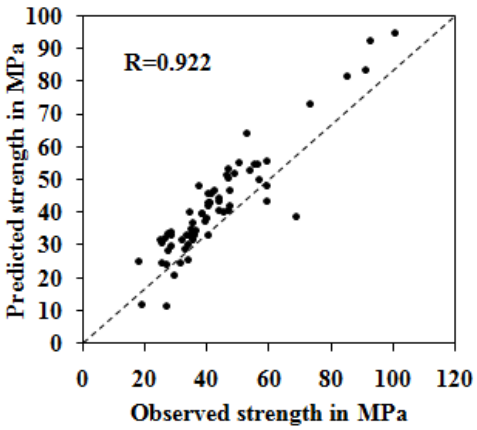

Fig. 5. Scatter plot for ANN2-2.

28 day strength of concrete is affected due to the water binder ratio (W/B) & increase in W/B can decrease the strength. Also replacement ratio of RA or Fly ash in concrete can decrease the strength of concrete (Shetty, 2005; Neville, 2012). Specifically in RAC, in a given mix when Aggregate to cement ratio increases, the strength decreases. Also increase in the CS can be seen with increase in water to total materials ratio and fine aggregate to total aggregate content up to a certain limit and further it shows a decrease in strength (Deshpande, 2016).

4.2. Model formulation using MGGP

With input parameters as mix proportions of concrete, properties of materials and non-dimensional parameters, models were calibrated using MGGP as shown in Table 1 and Table 2. Performance of each of the model in testing is shown in Table 9.

To find the optimal model, the MGGP algorithm was run several times with different combinations of the parameters as shown in Table 6. Results of models with Population:1000, generation:500, tree depth:4 and no. of genes:6 were found to be satisfactory and recorded here. Fig. 7 and Table 10 show the individual genes/model terms for the best models of MGGP1-1 and MGGP2-1 that were obtained during the conducted runs.

Each gene includes its weighing coefficient. It is seen that the weight of the genes (sub-programs) 1, 3, 5 and the bias terms are higher than the other genes for MGGP2-1 and high importance of gene 6, 4, 3 and bias term in MGGP1-1. This means that they have higher contribution to the strength prediction of concrete. Fig. 8 shows the expressional trees for the best models that were obtained during the conducted runs for MGGP3-1. Each gene includes its weighing coefficient. As can be observed from Fig. 8, the derived model is composed of complicated array of operators, variables, and constants to estimate the 28 CS of concrete.

Table 9. Performance of models developed using MGGP.

Set. No	Model No.	*RMSE* (m/s)	*MAE* (m/s)	*E*	*AARE*	*r*
1	MGGP 1-1	6.9110	5.5560	0.8262	14.3747	0.9090
	MGGP 1-2	8.5412	6.3821	0.7375	16.4551	0.8588
2	MGGP 2-1	4.0559	2.8832	0.8222	9.0642	0.9283
	MGGP 2-2	3.6216	2.8611	0.8649	9.6019	0.9414
3	MGGP 3-1	6.9458	5.3300	0.8244	13.3762	0.9095
	MGGP 3-2	8.4083	6.4100	0.7427	16.4922	0.8647
4	MGGP 4-1	4.2349	2.8108	0.8003	9.7842	0.9177
	MGGP 4-2	3.5550	2.7290	0.8824	10.3964	0.9518

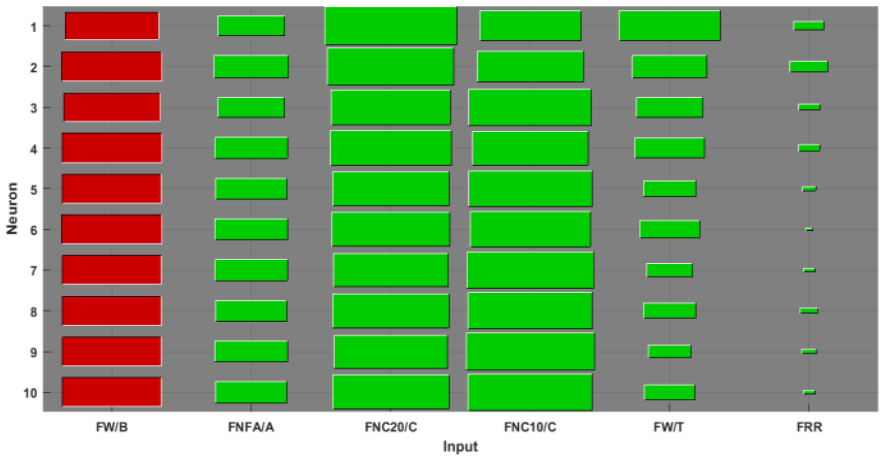

Fig. 6. Hinton diagram for ANN4-2.

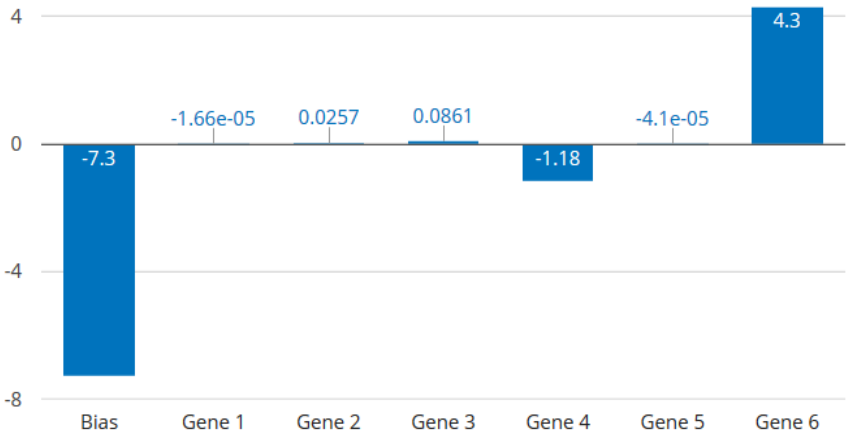

Fig. 7. Weights of the genes (sub-programs) of MGGP1-1.

Table 10. Individual genes/model terms for the prediction of CS for MGGP2-1.

Term	Value
Bias	14.5
Gene 1	$(1.2\ x_1^2)\ /\ (x_6 - 1.0\ x_7)$
Gene 2	$-(0.0139\ x_1^2\ x_7)\ /\ (x_6 + x_7)$
Gene 3	$-(1.16\ x_1^2)\ /\ (x_6 + x_7)$
Gene 4	$(0.00531\ x_2\ x_5)\ /\ (\text{psqroot}(x_6) + \text{psqroot}(x_7))$
Gene 5	$-(9.19\ x_2\ x_5)\ /\ x_6 + 5.08)^2$
Gene 6	$-\left(0.00149\ (x_3 + x_7)\ (x_3 + x_6 + \text{psqroot}(x_6))\right)\ /\ (2.0\ x_2 + x_6)$

Each gene includes its weighing coefficient. It is seen that the weight of the genes (sub-programs) 1, 3, 5 and the bias terms are higher than the other genes for MGGP2-1 and high importance of gene 6, 4, 3 and bias term in MGGP1-1. This means that they have higher contribution to the strength prediction of concrete. Fig. 8 shows the expressional trees for the best models that were obtained during the conducted runs for MGGP3-1. Each gene includes its weighing coefficient. As can be observed from Fig. 8, the derived model is composed of complicated array of operators, variables, and constants to estimate the 28 CS of concrete.

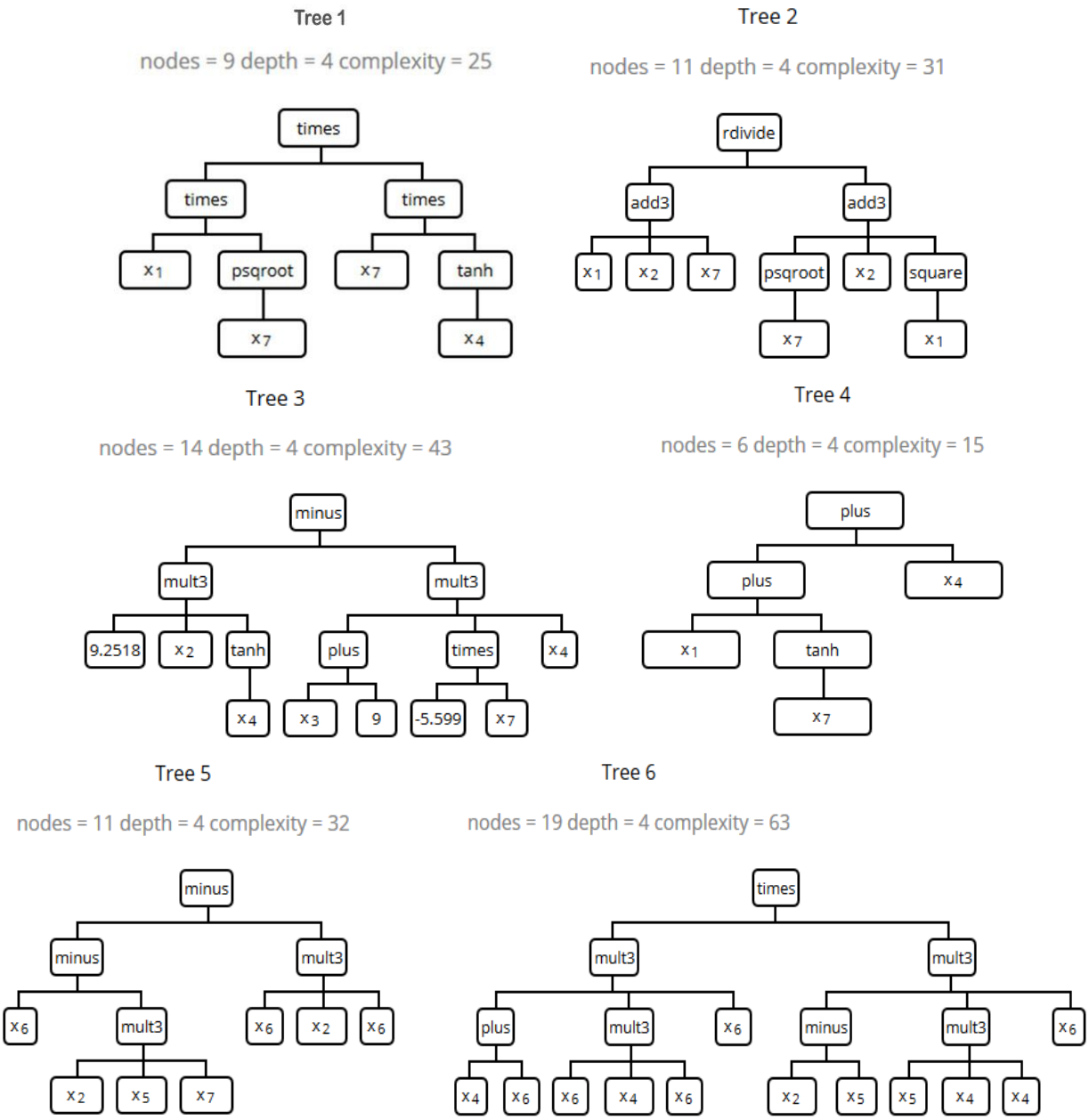

Fig. 8. Expression trees of the best models for the prediction of CS of concrete for MGG 3-1.

To facilitate the use of the developed model, model MGGP3-1 was transformed into a simplified functional form (Eq. (6)):

$$
\begin{aligned}
y \;=\; & 16.9\,x_6 - 94.0\,x_4 - 94.0\,x_1 - 94.0\tanh(x_7) - \\
& (1.0\,(7.79e^{15}\,x_1 + 7.79e^{15}\,x_2 + 7.79e15\,x_7)) \,/ \\
& (1.76e^{13}\,x_2 + 1.76e^{13}\cdot \mathrm{sqrt}(x_7) + 1.76e^{13}\,x_1^2) - \\
& 16.9\,x_2\,x_6^2 + 153.0\,x_2\tanh(x_4) + 92.9\,x4\,x7\,(x_3 + 9.0) - \\
& 16.9\,x_2\,x_5\,x_7 - 4988.0\,x_1\,x_7\cdot \mathrm{sqrt}(x_7)\tanh(x_4) + \\
& 995.0\,x_4^3\,x_5\,x_6^4\,(x_4 + x_6)\,(x_2 - 1.0\,x_5) + 550.0
\end{aligned}
\tag{6}
$$

where x_1=RWC, x_2=RNFA/A, x_3=RNC20/C, x_4= RNC10/C, x_5=RC20/C, x_6=RC10/C, x_7=RW/T.

Fig. 9 presents the accuracy against the complexity of the evolved models. Green dots represent the Pareto front of models in terms of model performance ($1 - R^2$) and model complexity. Blue dots represent non-Pareto models. The red circled dot represents the best model in the population in terms of $R2$ on the training data (Searson, 2015). The red circle in Fig. 10 for MGGP3-1 designates the best model presented herein that is not outperformed by any other model in terms of complexity and fitness. A less complex model for MGGP2-1 can be seen in Fig. 9.

From the Pareto front (Figs. 9 and 10), user can decide whether the incremental gain in performance is worth with associated model complexity. Concisely, the MGGP paradigm evolves multiple models which provide more number of choices to the designer. A single model can be selected based on the application requirements (Searson et al., 2007; Pandey, 2015). Figs. 11 and 12 also depict the convergence characteristics of the genetic programming algorithm.

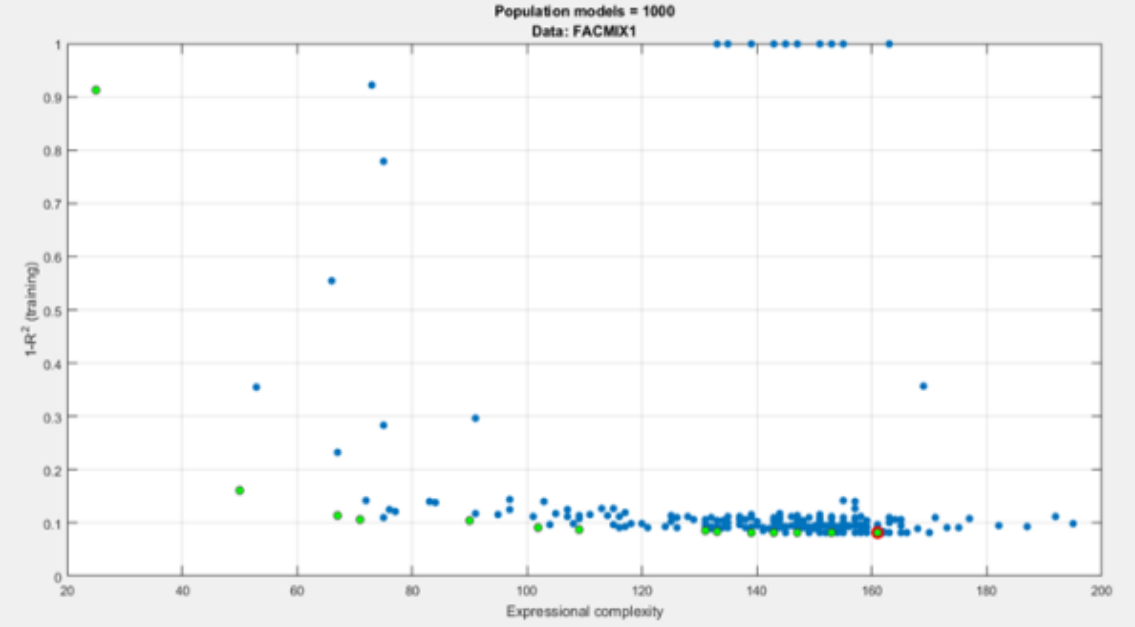

Fig. 9. Pareto front report for MGGP2-1.

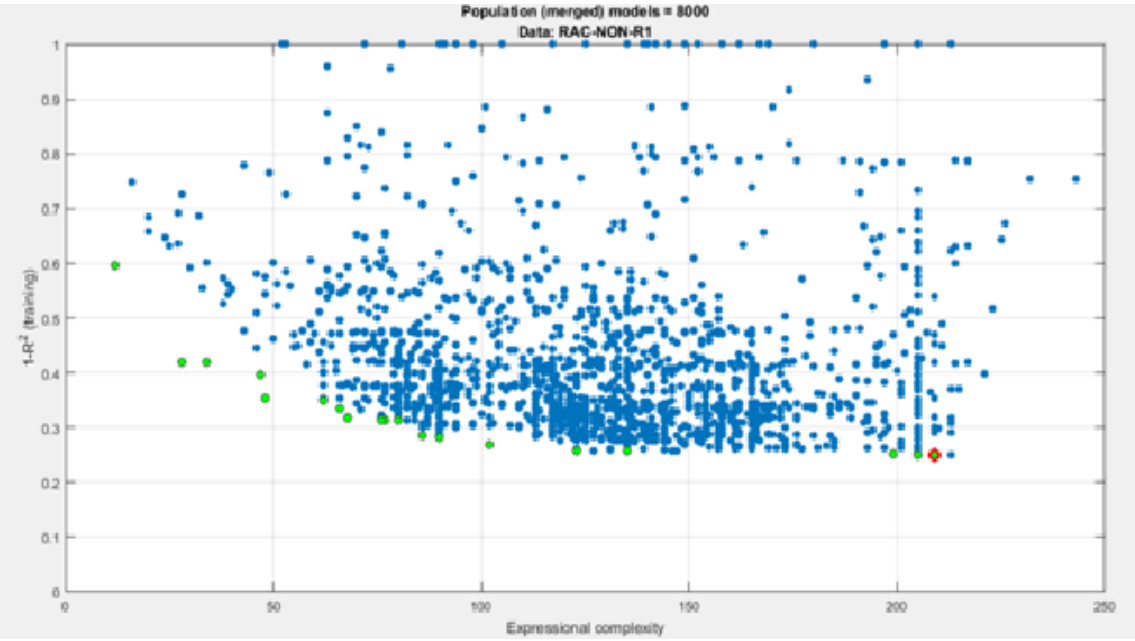

Fig. 10. Pareto front report for MGGP3-1.

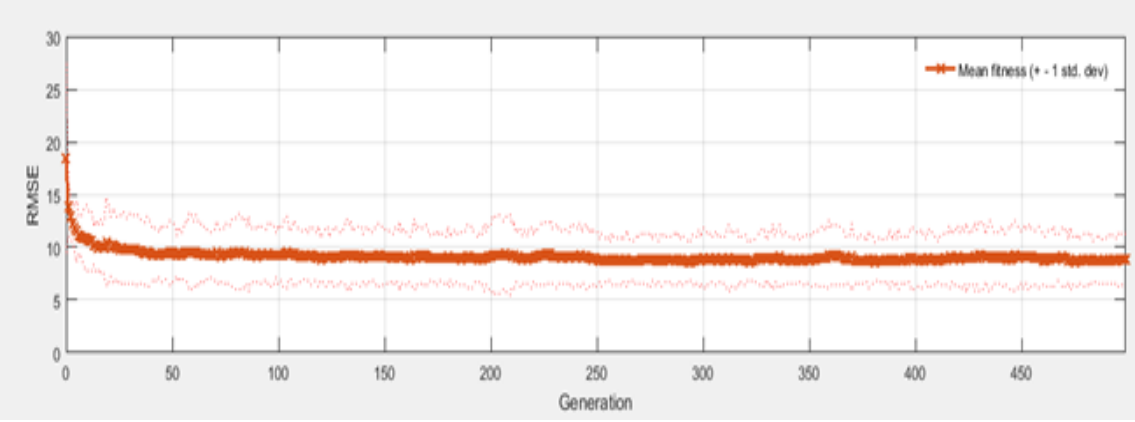

Fig. 11. Convergence of the MGGP solutions for MGGP1-2.

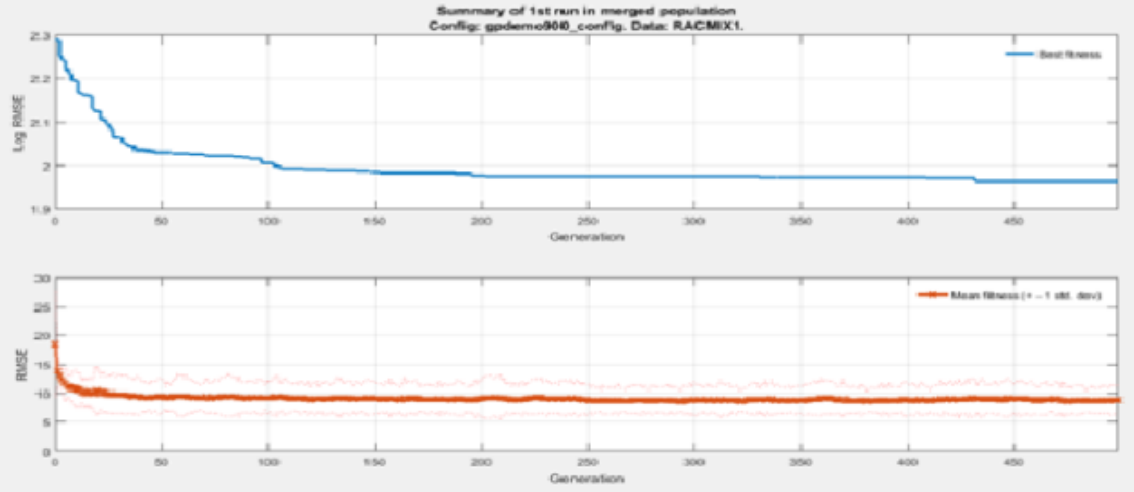

Fig. 12. Convergence of the MGGP solutions for MGGP3-2.

It is evident that the mean fitness of the curve becomes smoother after 100 (in both the figures) generations and that the change in objective function is not significant near the end of the genetic programming run. It indicates that running the genetic programming for more generations does not result in a more favorable outcome. However, as the best fitness is reported at 450 (RMSE-7.14 for MGGP1-2) in this particular case, it suggests that the genetic programming algorithm should have to run for at least 500 generations for all the models developed here. Figs. 13-16 show the frequency of input data for models in GP with coefficient of determination $R^2 \geq 0.6$ (Searson, 2010; Searson et al., 2007; Pandey, 2015). Input frequency of the graphical input frequency analysis of single model or of a user specified fraction of the population is used to provide the identification of Input variables that are significant to the output (Searson et al., 2007; Singh, 2014).

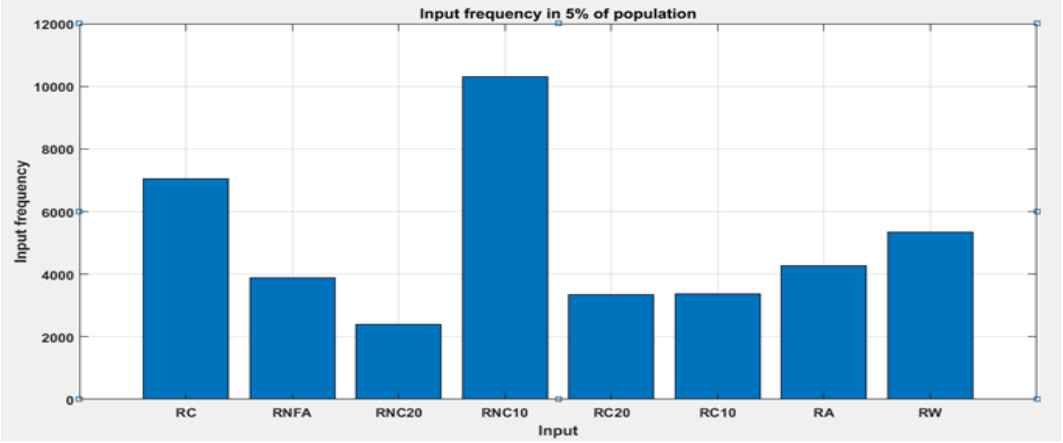

Fig. 13. Input frequency for MGGP1-1.

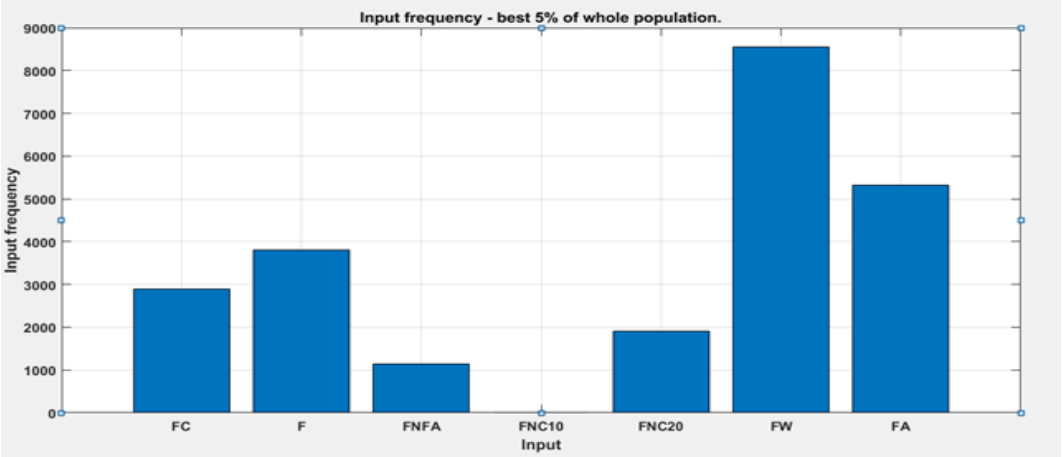

Fig. 14. Input frequency for MGGP2-1.

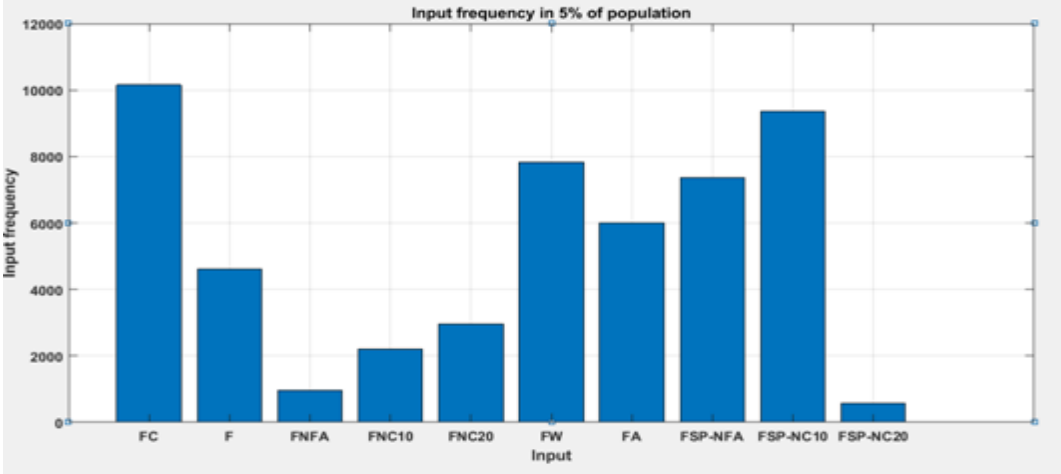

Fig. 15. Input frequency for MGGP2-2.

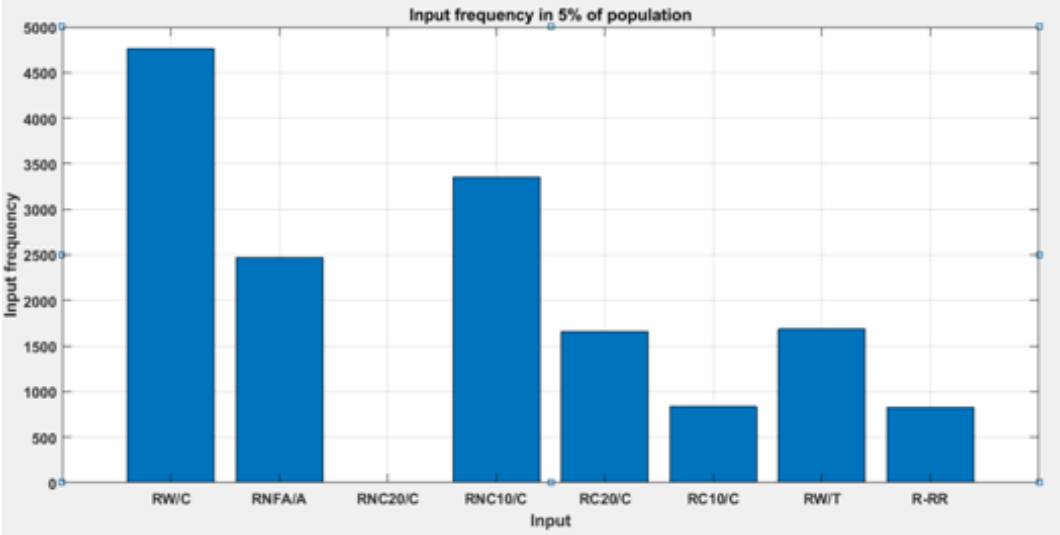

Fig. 16. Input frequency for MGGP3-2.

For MGGP1-1, out of 8 parameters, parameters: RNC10, RC and RW are influential followed by RNFA, RA, RC20, RC10 and RNC20 content. This finding is in tune with the fundamental knowledge of concrete technology (Shetty, 2005; Neville, 2012). For MGGP2-1, FW and F are seen as important parameters. With addition of properties of materials like Specific gravity of aggregate content, MGGP2-2 shows specific gravity as an influential parameter with cement content being the most influential parameter followed by water content and other parameters. In MGGP3-2 the frequency of input parameters is as shown in figure 16 which shows RC20/C as the least influential parameter.

4.3. Models developed using MT

Model tree is the third technique used to predict the 28 day strength of concrete. Fig. 17 below shows a typical Model Tree developed for Model 1-1. The linear regression equations developed by MT1-1 are shown in Fig. 18.

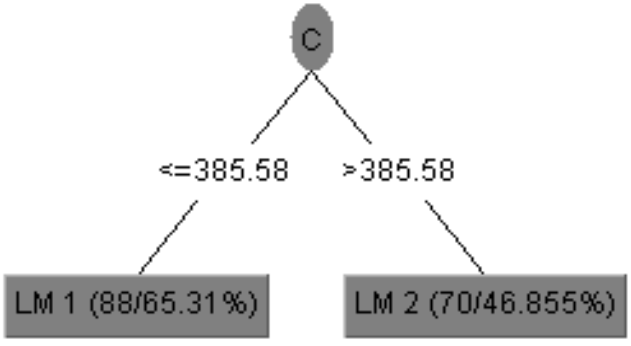

Fig. 17. Model Tree for MT1-1.
(The first number in the bracket is the number of samples in the subset sorted to this leave and the second one-root mean squared error (*RMSE*) of the corresponding linear model divided by the standard deviation of the samples subset for which it is built.) (expressed in percent)

```
Scheme:     weka.classifiers.trees.M5P -M 4.0
Relation:   RACData2-MT-TRAINING
Instances:  158
Attributes: 9
            C, NFA, NC-20, NC-10, RC-20, RC-10, A, W, S
=== Classifier model (full training set) ===
M5 pruned model tree: (using smoothed linear models)

C <= 385.58 : LM1 (88/65.31%)
C > 385.58 : LM2 (70/46.855%)

LM num: 1
S = 0.0142 * C - 0.002 * NFA - 0.0039 * NC-20 + 0.0172 * NC-10 - 0.0048 * RC-20
    - 0.0118 * RC-10 + 0.8318 * A - 0.0365 * W + 39.8858

LM num: 2
S = 0.0912 * C - 0.022 * NFA - 0.0047 * NC-20 + 0.0485 * NC-10 - 0.0058 * RC-20
    - 0.0044 * RC-10 - 0.3575 * W + 93.4442

Number of Rules : 2

Time taken to build model: 0.26 seconds
```

Fig. 18. Equations developed for MT1-1.

Similarly for other models, the number of equations developed are shown in Table 7. Equation developed for MT1-1 as shown in Fig. 17, shows positive coefficients to cement content, admixture content and RC-10 content.

Negative coefficients can be seen for other parameters specially water content, indicating that its increase in mix after a certain limit can decrease the strength of concrete which agrees with the domain knowledge (Shetty, 2005; Neville, 2012; Deshpande, 2016). This can also be seen in MT equation developed for Fly ash based concrete i.e Model MGGP2-1. The series of equations developed for MT2-1 areas shown in Fig. 17. Inclusion of replacement ratio in models for RAC and Fly ash based concrete in Model 3-2 and 4-2 are shown in Fig. 19 for RAC and Fig. 20 or Fly ash based concrete.

The performance of each model developed using MT in each set are as shown in Table 11.

```
Scheme:     weka.classifiers.trees.M5P -M 4.0
Relation:   RACR2-TRAINING
Instances:  159
Attributes: 9
            W/C, NFA/A, RNC20/C, RNC10/C, RC20/C, RC10/C, RW/T, R-RR, RCS
Test mode:  evaluate on training data
M5 pruned model tree: (using smoothed linear models)
W/C <= 0.452 : LM1 (62/57.194%) and W/C > 0.452 : LM2 (97/69.324%)
LM num: 1
RCS = -119.3856 * W/C + 2.2316 * NFA/A + 8.3196 * RNC10/C - 3.2418 * RC20/C + 27.2358
      * RW/T + 99.9119
LM num: 2
RCS = -12.915 * W/C + 1.5343 * NFA/A - 3.8624 * RNC20/C + 1.4344 * RNC10/C - 5.5796 *
      RC20/C - 6.1185 * RC10/C + 18.7246 * RW/T + 53.5031
Number of Rules : 2
```

Fig. 19. Equations developed for MT3-2.

```
Scheme:     weka.classifiers.trees.M5P -M 4.0
Relation:   NON-FAC-MD4-ANN-MT-TRAINING
Instances:  79
Attributes: 7
            FW/B , FNFA/A , FNC20/C, FNC10/C, FW/T, F-RR, FCS
Test mode:  user supplied test set: size unknown (reading incrementally)
=== Classifier model (full training set) ===
M5 pruned model tree:
(using smoothed linear models)
LM1 (79/39.428%)
LM num: 1
FCS = -66.8101 * FW/B - 50.6429 * FNFA/A - 3.9907 * FNC20/C - 2.9493 * FNC10/C
      - 0.167 *F RR + 103.5807
Number of Rules : 1
```

Fig. 20. Equations developed for MT4-2.

Table 11. Performance of models developed using MT.

Set. No	Model No.	*RMSE* (m/s)	*MAE* (m/s)	*E*	*AARE*	*r*
1	MT 1-1	10.66	7.213	0.586	17.123	0.767
	MT 1-2	9.883	6.176	0.706	14.011	0.843
2	MT 2-1	4.544	3.442	0.77	10.916	0.902
	MT 2-2	4.641	3.861	0.797	11.284	0.929
3	MT 3-1	10.66	7.212	0.586	17.122	0.767
	MT 3-2	10.66	7.212	0.586	17.122	0.767
4	MT 4-1	8.053	3.992	0.278	15.326	0.795
	MT 4-2	6.944	3.987	0.463	14.917	0.817

4.4. Comparison of models developed using ANN, MGGP and MT

The models were developed using same data division and their results were compared on testing data sets as shown in Tables 8, 9 and 11. Performance of each of the model was judged using 5 statistical error measures namely *RMSE*, *MAE*, *E*, *AARE* and *r*.

ANN outperformed the other data driven techniques as seen in the Tables 8, 9 and 11. ANN predicted the output of 28 day CS of concrete better, as compared to MGGP and MT. Figs. 21and 22 show the predictions of RAC and Fly ash based concrete in models 1 in Set 1 and Set 2.

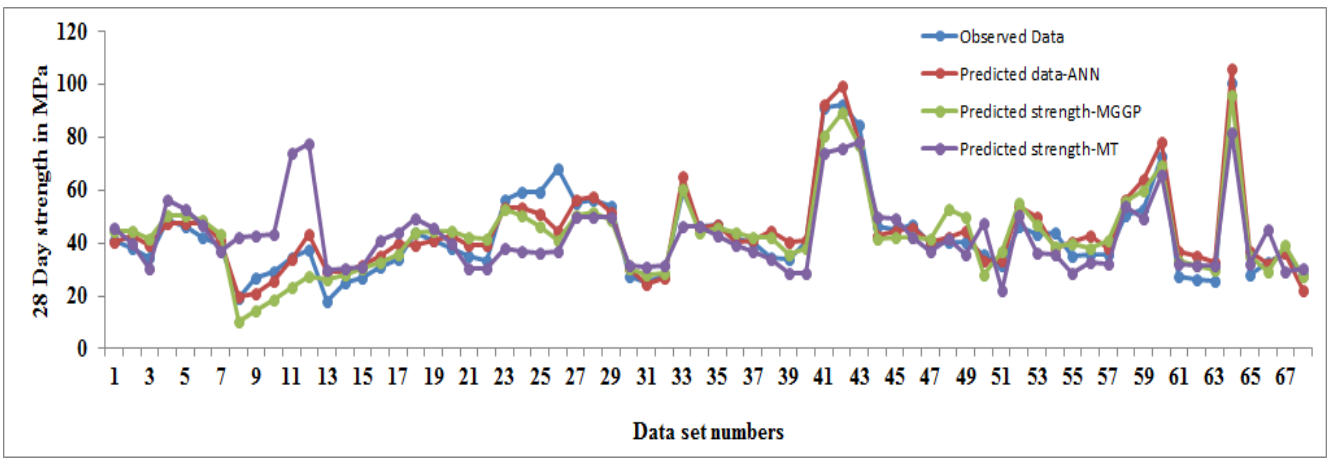

Fig. 21. Prediction trend for model 1-1.

Fig. 22. Prediction trend for model 2-1.

On the other hand, MGGP model performs better than MT models. Table 8 shows that the performance of model ANN1-1 is better as compared to ANN1-2. This can be also be seen in models developed using MGGP. Models developed using kg/m^3 proportions of materials predict strength better as compared to models developed with additional properties of materials i.e water absorption of aggregates in Set 1 in ANN. A similar performance can be seen with models developed using MGGP when Specific gravity of MNFA, FNCA20 and FNC10 become part of input parameters in Set 2. Presence of non-dimensional parameters as input parameters for development of models using ANN, MGGP and MT show a similar performance in RAC and fly ash based concrete. Scatter plots for ANN1-1 and MGGP1-1 are as shown in Figs. 23 and 24, respectively. Scatter plot for MGGP1-1 shows slight under prediction of RAC.

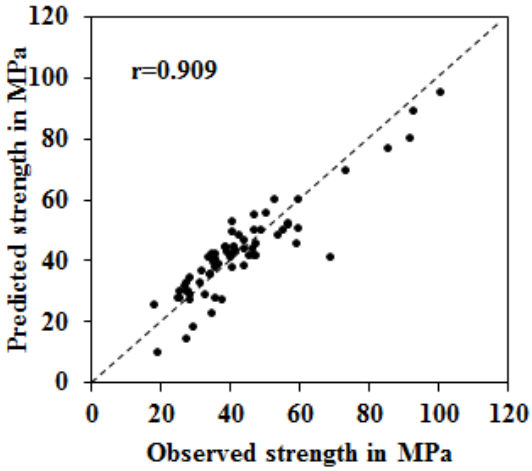

Fig. 23. Scatter plot for MGGP 1-1.

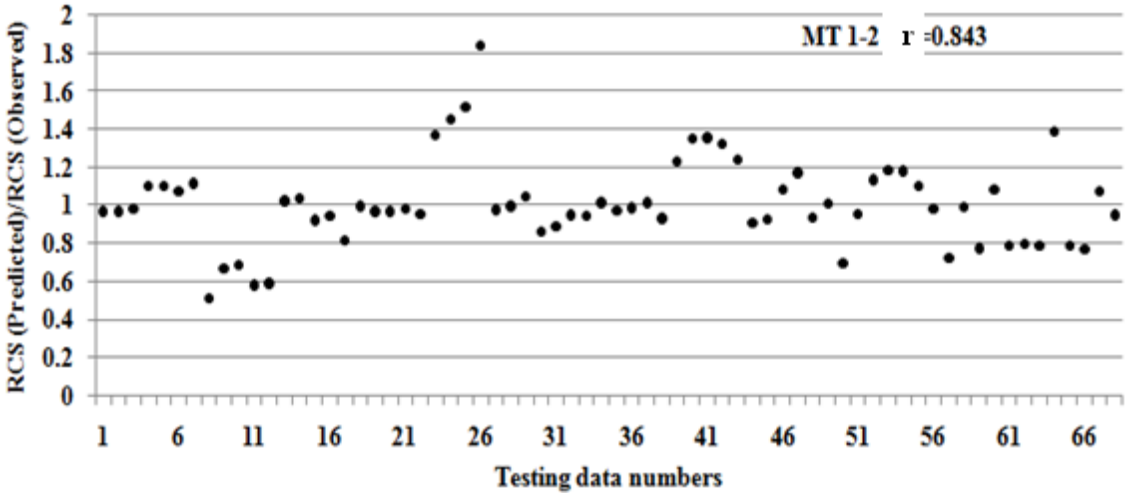

Fig. 24. Observed and Predicted values for MT 1-2.

However models in Set 1 and Set 2 developed using MT show performance of models with properties of materials better than relative proportions of materials i.e than MT1-1. This can be seen through lower *r*, *E* and higher *AARE* values for MT1-1. The same can be seen with models developed with fly ash based concrete too. The plot in Fig. 24 shows the trend of RAC prediction and observed for MT1-2. This figure shows the ratio of the predicted to observed RAC strength values. Apparently, a ratio closer to 1 indicates a more precise prediction.

Non-dimensional parameters have a greater significance in ascertaining strength characteristics of concrete. It has also been seen that instead of using proportions of materials as input parameters, if individual non-dimensional parameters are used, the performance of

the models can be similar as that of the former or increases (Deshpande, 2014). Thus Set 3 and Set 4 were designed with non-dimensional parameters as input parameters. It was seen that with higher *r*, *AARE* and *E* values, models with non-dimensional parameters perform better when developed using ANN. A slight decrease in the performance of model ANN3-2 can be seen as compared to ANN3-1 in which *RR* was an additional parameter included. Thus it can be said that the influence of *R-RR* parameter is considered in the parameter: aggregate proportion. Similar performance can be seen in fly ash based concrete (model ANN4-1 and ANN4-2). MGGP3-1 shows a similar performance as MGGP1-1 and with *R-RR* as input parameter in MGGP3-2 shows *r* as 0.864. An increased (*r*=0.952) performance can be seen in MGGP4-2 as compared to MGGP4-1 (*r*=0.918).

Models developed using MT for RAC i.e MT3-1 and MT3-2 showed a similar performance. MT4-2 shows an increase in performance when *F-RR* was considered as an input parameter as compared to MT4-1.

Thus it can be said that models developed using ANN and MGGP displayed a good performance with relative proportions of constituents of materials in concrete; Non-dimensional parameters as input parameters performed similarly or slightly better than the model with proportions of materials as input parameters, however it is necessary to select non-dimensional parameters judiciously for a better representation of material proportions. Models developed using MT performed poor as compared to ANN and MGGP, however they have an advantage of series of equations which can be readily used. In the Hinton diagram for ANN1-1, RNC20, RW and RC are influential factors followed by other parameters. A similar trend of influential parameters can be seen in MGGP1-1 as well. A similar trend in terms of coefficients can be seen in model MT1-1 developed using MT (refer Fig. 19). Similarly for models ANN2-1, MGGP2-1 and MT2-1 with cement and fly ash content and specific gravity of fine aggregate are the most important parameters followed by other parameters. Parameter SP-NC20 was eliminated from MT models and seen as very low influence in ANN and MGGP models.

With non -dimensional parameters as input parameters, the influential parameters in ANN3-1, MGGP3-1 and MT3-1 are as shown in Figs. 25, 26 and 27, respectively. A slight difference in the influential parameters can be seen. ANN builds an approximate function that matches a list of inputs to the desired outputs. In the process, it adjusts the weights and biases to reach a predefined goal. This process makes ANN flexible and increases its performance as compared to GP.

GP, on the other hand, is based on evolutionary approach technique in which it does not involve any transfer function and evolves generations of 'offspring' based on the 'fitness criteria' and genetic operations. GP approach works with the concept of disregarding input parameters that do not contribute effectively in the model and thus based solely on 'fitness' criteria. In the process of building programs (through processes of mutation, crossover and reproduction), GP selects parameters which are useful in achieving the fitness criteria and deletes the remaining. This can reduce the - performance of GP as compared to ANN. This is in contrast to the work done by Londhe (2008). However the work in Londhe (2008), the problems were indeterministic in nature; whereas predicting strength of concrete is of deterministic nature. This may be the reason behind ANN working better than GP. However this needs to be explored further.

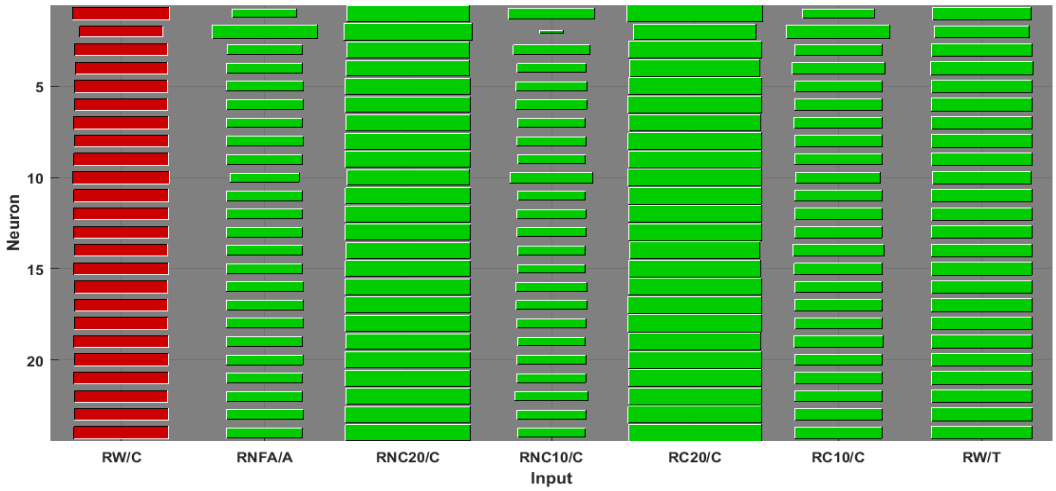

Fig. 25. Hinton diagram for ANN3-1.

In Model tree with M5P algorithm, the basic tree is formed based on a splitting criterion. It uses the standard deviation of the class values for each node as a measure of the error at that node and then calculates the expected error reduction as a result of testing each attribute at that node. Then, the attribute that maximizes the expected error reduction is selected to split the data at that node and the remaining are not considered in the developed equation. Thus RC10/C is included in Eq. (2) of MT3-2 and excluded in equation 1 of MT3-2 (refer Fig. 27). This can also be one of the reasons for poorer performance of MT as compared to ANN and MGGP. The errors of a good prediction model should be independent of physical parameters involved in that problem. Otherwise, it can be concluded that those physical parameters should be added to that prediction model or they weren't

considered correctly in that model. It should be mentioned that the errors of developed models in set 3 and 4, show a similar or increased performance when RR is included as input parameter in ANN, MT and MGGP, except for model MGGP3-2. However the authors recommend the use of individual aggregate ratios as they display a better picture about contribution of each aggregate type on the strength of concrete. Thus it can be seen that models developed using ANN, MGGP and MT learn from the examples given and predict the strength of concrete with influential parameters which are in tune with the domain knowledge. The correlation of input parameters and output parameters seen in Tables 1, 2 and 3 also show significant parameters as cement content followed by water and aggregates for the current study.

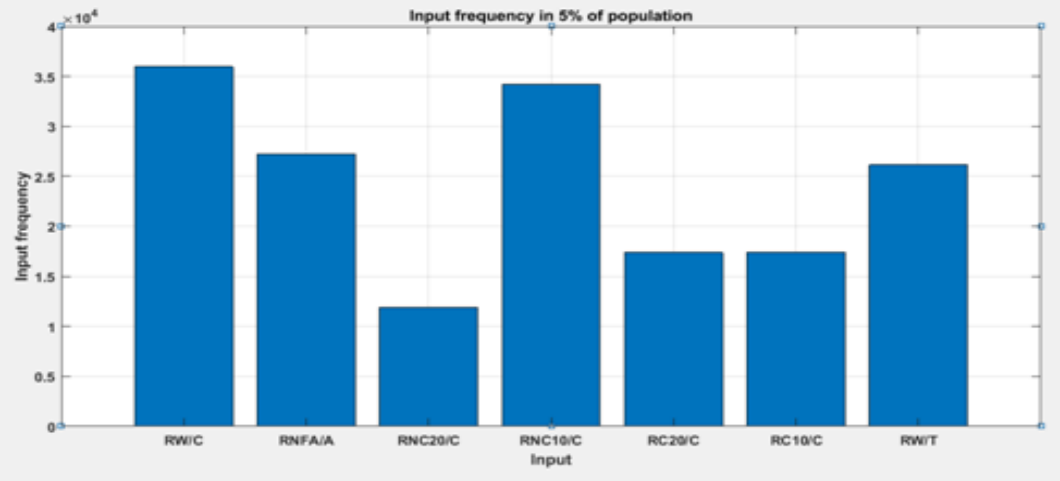

Fig. 26. Input frequency for MGGP3-1.

```
M5 pruned model tree:
(using smoothed linear models)

RW/C <= 0.452 : LM1 (62/57.016%)
RW/C >  0.452 : LM2 (96/69.464%)

LM num: 1
RCS =
        -119.4165 * RW/C
        + 2.2235 * RNFA/A
        + 8.3283 * RNC10/C
        - 3.2418 * RC20/C
        + 27.9404 * RW/T
        + 99.8744

LM num: 2
RCS =
        -13.0527 * RW/C
        + 1.5424 * RNFA/A
        - 3.8705 * RNC20/C
        + 1.4534 * RNC10/C
        - 5.587 * RC20/C
        - 6.1269 * RC10/C
        + 19.3821 * RW/T
        + 53.5492
```

Fig. 27. Equations for MT3-1.

Thus, models developed using ANN technique perform better as compared to MGGP and MT. MGGP on other hand perform better than MT. This can be seen in case of RAC and fly ash based concrete and different properties of materials. ANN though performs better; has a limitation of its ease of its use. MGGP and MT on other hand are easy to use with equation and series of equations developed respectively for ready use. Performance of MGGP and MT though less as compared to ANN, equations are developed by the techniques by understanding the basics of domain knowledge which can be seen through the equations.

5. Conclusions

In the current study an attempt was made to predict 28 day compressive strength of Recycled Aggregate concrete and Fly ash based concrete with input parameters as kg/m^3 proportions of materials used in concrete, properties of materials used and non-dimensional parameters. The following outcomes can be noted from the current study:

- Models developed using ANN outperform MGGP and MT models with higher *R, AARE* and *E* values and lower RMSE and MAE values.
- ANN has an advantage of better performance; MGGP on other hand with acceptable accuracy can provide equations which can be readily used. Models developed using MT display performance less as compared to ANN and MGGP.
- Use of relative proportions of materials as input parameters predicts strength better than input parameters with properties of materials in ANN and MGGP. However MT shows performance with properties of materials better as compared to relative proportions of materials.
- Use of Non- dimensional parameters as input parameters can be encouraged for prediction of CS of concrete; however judicious selection of non-dimensional parameters needs to be done.

The study also shows that ANN, MGGP and MT learn from the examples given and display influential input parameters which are in tune with the domain knowledge of Concrete Technology specifically for ANN. GP and MT show a slight variation as compared to influential parameters observed in ANN and maybe due to the basic working concept of MGGP and MT.

References

Adnan SH, Rahman I.A, Saman HM (2011). Recycled aggregate as coarse aggregate replacement in concrete mixes. *ASEAN Australian Engineering Congress 2011*, Kuching, Sarawak, Malaysia, 2011.

Adriana TAD, Monica BL, Koji de JN (2013). Prediction of compressive strength of concrete containing construction and demolition waste using artificial neural networks. *Construction and Building materials*, 38, 717-722.

Agarwal SD, Karnnkal AB, Patil PN (2011). Feasibility study of use of RCA in concrete. *International Journal of Research in Engineering Sciences and Technology*, SP-II, 70-75.

Ahmet OZ, Murat PB, Erdogan O, Erdog K, Naci C, Bhatti A (2006). Predicting the compressive strength and slump of high strength concrete using neural network. *Construction and Building Materials*, 20, 769–775.

Bayazidi BM, Wang GG, Amir H, Alavi H, Gandomi AH (2014). Multigene genetic programming for estimation of elastic modulus of concrete. *Mathematical Problems in Engineering,* 2014, 1-10.

ChakradharaRao M, Bhattacharyya SK, Barai SV (2010). Influence of field recycled coarse aggregate on properties of concrete, *Materials and Structures*, 44(1), 205-220.

Corinaldesi V (2010). Mechanical and elastic behavior of concretes made of recycled-concrete coarse aggregates. *Construction and Building Materials*, 24, 1616–1620.

Dapena E, Alaejos P, Lobet A, Pérez D (2011). Effect of recycled sand content on characteristics of mortars and concretes. *Journal of Materials in Civil Engineering*, 23(4), 414-422.

David RL, Gregory JJr (1999). Evaluating the use of "goodness of fit" measures in hydrological and hydro climatic model validation. *Water Resources Research*, 35(1), 233-241.

Deepa C, SathiyaKumari K, Sudha KP (2010). Prediction of the compressive strength of high performance concrete mix using tree based modeling. *International Journal of Computer Applications*, 6(5), 18–24.

Deshpande N (2016). Study of Properties of Concrete Made with Recycled Aggregate and Industrial Wastes with Special Application to Housing. *Ph.D thesis*, Shivaji University.

Deshpande N, Londhe SN, Kulkarni SS (2014). Modeling compressive strength of recycled aggregate concrete by Artificial Neural Network, Model Tree and Non-linear Regression. *International Journal of Sustainable Built Environment*, 3, 187–198.

Dias WPS, Pooliyadda SP. (2001). Neural networks for predicting properties of concretes with admixtures. *Construction and Building Materials*, 15, 371-379.

Domingo-Cabo A, Lázaro C, López-Gayarre C, Serrano-López MA, Serna P, Castaño-Tabares JO (2009). Creep and shrinkage of recycled aggregate concrete. *Construction and Building Materials*, 23, 2545–2553.

Duan ZH, Kou SC, Poon CS. (2013). Prediction of compressive strength of recycled aggregate concrete using artificial neural networks. *Construction and Building Materials*, 40, 1200–1206.

Evangelista L, Brito JCde (2010). Durability performance of concrete made with fine recycled concrete aggregates. *Cement & Concrete Composites,* 32, 9–14.

Evangelista LR, Brito JCde (2004). Criteria for the use of fine recycled concrete aggregates in concrete production. *International RILEM Conference on Use of Recycled Building Materials in Building and Structures*, 8-11 Nov 2004, Barcelona, Spain.

Fathifazl G, Abbas A, Razaqpur AG, Isgor OB, Fournier B, Foo S (2009). New mixture proportioning method for concrete made with coarse recycled concrete aggregate. *Journal of Materials in Civil Engineering*, 21(10), 601-611.

Frank E, Mark A, Hall Ian, Witten H (2016). The WEKA Workbench. Fourth Edition. *Online Appendix for Data Mining: Practical Machine Learning Tools and Techniques.* Morgan Kaufmann.

Goncalves A, Esteves A, Vieria M (2004). Influence of recycled concrete aggregates on concrete durability. *International RILEM Conference on Use of Recycled Building Materials in Building and Structures*, 8-11 Nov 2004, Barcelona, Spain.

Gorphade VH, Sudarsana Rao H, Beulah M (2014). Development of genetic algorithm based neural network model for predicting workability and strength of high performance concrete. *International Journal of Inventive Engineering and Sciences (IJIES),* 2(6), 1-8.

Gupta R, Kewalramani MA, Goel A (2004). Prediction of concrete strength using neural-expert system. *Journal of Materials in Civil Engineering*, 18(3), 462-466.

Hansen TC, Narud H (1983). Strength of recycled concrete made from crushed concrete coarse aggregate. *Concrete des Constr,* 5(1), 79-83.

I-Cheng Y (2007). Modeling slump flow of concrete using second-order regressions and artificial neural networks. *Cement & Concrete Composites*, 29, 474–480.

Jain A, KumarJha S, Misra S (2008). Modeling and Analysis of concrete slump using Artificial Neural Networks. *Journal of materials in Civil engineering*, 20(9), 628-633.

Jong-In KM, Kim DK, Maria MQ, Feng M, Yazdani F (2004). Application of Neural Networks for Estimation of Concrete Strength. *Journal of Materials in Civil Engineering*, May/June 2004, 257-264.

Khatib JM (2005). Properties of concrete incorporating fine recycled aggregate. *Cement Concrete Research,* 35(4), 763-769.

Konin A, Kouadio DM (2011). Influence of cement content on Recycled aggregates concrete properties. *Modern Applied Science*, 5(1), 23-31.

Kotrayothar D (2012). Recycled Aggregate Concrete for Structural Applications. *Ph.D thesis,* University of Western Sydney.

Kou S (2006). Reusing Recycled Aggregates in Structural Concrete. *Ph.D thesis,* Hong Kong Polytechnic University.

Kumutha R, Vijai K (2010). Strength of concrete incorporating aggregates recycled from demolition waste. *ARPN Journal of Engineering and Applied Sciences*, 5(5). 64-71.

Londhe SN (2008). Soft computing approach for real-time estimation of missing wave heights. *Ocean Engineering*, 35, 1080–1089.

Londhe SN, Dixit PR (2012). Genetic Programming: A Novel Computing Approach in Modeling Water Flows Genetic Programming – New Approaches and Successful Applications. Chapter 9, InTech.

Maier H, Dandy G (2000). Neural networks for the prediction and forecasting of water resources variables: a review of modelling issues and applications. *Environmental Modeling & Software*, 15(1), 101-124.

Neville AM (2012). Properties of Concrete. Pearson Education, USA and UK.

Ni HG, Wang JZ (2000). Prediction of compressive strength of concrete by neural networks. *Cement and Concrete Research*, 30, 1245-1250.

Nikoo M, Torabian Moghadam F, Sadowski A (2015). Prediction of concrete compressive strength by evolutionary artificial neural networks. *Advances in Materials Science and Engineering,* 2015, 1-8.

Padmini AK, Ramamurthy K, Matthews MS (2003). Relative moisture movement through recycled aggregate concrete. *Cement and Concrete Research*, 54(5), 377-384.

Pandey DS, Pan I, Das S, Leahy JJ, Kwapinski W (2015). Multi-gene genetic programming based predictive models for municipal solid waste gasification in a fluidized bed gasifier. *Bioresource Technology*, 179, 524–533.

Pelufo M J, Domingo A, Ulloa VA, Vergara NN (2009). Analysis of moisture state of recycled coarse aggregate and its influence on compression strength of the concrete. *Proceedings of the International Association for Shell and Spatial Structures (IASS) Symposium 2009, Valencia Evolution and Trends in Design, Analysis and Construction of Shell and Spatial Structures,* 28 September–2 October 2009, Universidad Politecnica de Valencia, Spain

Pereira P, Evangelista L, Brito Jde (2012). The effect of superplasticisers on the workability and compressive strength of concrete made with fine recycled concrete aggregates. *Construction and Building Materials*, 28, 722–729.

Poon CS, Kou SC, Lam L (2007). Influence of recycled aggregate on slump and bleeding of fresh concrete. *Materials and Structures,* 40, 981–988.

Poon CS, Shui ZH, Lam L, Fok H, Kou SC (2004). Influence of moisture states of natural and recycled aggregates on the slump and compressive strength of concrete. *Cement and Concrete Research*, 34, 31–36.

Quinlan JR (1992). Learning with Continuous Classes. *In: Adams and Sterling, (Eds.). Proceedings of 5th Australian Joint Conference on Artificial Intelligence*. World Scientific, Singapore.

Ryu JS (2002). An experimental study on the effect of recycled aggregate on concrete properties. *Magazine of Concrete Research*, 54(1), 7-12.

Sarıdemir M (2010). Genetic programming approach for prediction of compressive strength of concretes containing rice husk ash. *Construction and Building Materials*, 24, 1911–1919.

Schoppe BM (2011). Shrinkage and modulus of elasticity in concrete with recycled aggregates. *M.Sc. thesis*, California Polytechnic State University.

Searson DP (2015). GPTIPS 2: an open-source software platform for symbolic data mining. Chapter 22 in Handbook of Genetic Programming Applications, A.H. Gandomi et al., (Eds.), Springer, New York, NY.

Searson DP, Leahy DE, Willis MJ (2010). GPTIPS: An open source genetic programming toolbox for multigene symbolic regression. *Proceedings of the International Multi Conference of Engineers and Computer Scientists 2010*, I, IMECS 2010, March 17-19, 2010, Hong Kong.

Searson DP, Willis MJ, Montague GA (2007). Co-evolution of non-linear PLS model components. *Journal of Chemometrics*, 2, 592-603.

Searson PD (2015). GPTIPS 2: An open-source software platform for symbolic data mining. Cornell University Library. DOI: arXiv:1412.4690

Shetty MS (2005). Concrete Technology. 17th edition. S. Chand and Company, New Delhi.

Singh HK (2014). Prediction of shear strength of deep beam using Genetic Programming. *B.Tech thesis*, National Institute of Technology, Rourkela, India.

The ASCE Task Committee (2000). Artificial Neural Networks in Hydrology I: Preliminary concepts. *Journal of Hydrologic Engineering,* 5(2), 115-123.

Yaprak H, Aruntas HY, Demir I, Simsek O, Durmus G (2011). Effects of the fine recycled concrete aggregates on the concrete properties. *International Journal of the Physical Science,* 6(10), 2455-2461.

Yong PC, Teo DCL (2009). Utilization of Recycled aggregate as coarse aggregate in concrete. *UNIMAS-E Journal of Civil Engineering*, 1(1), 1-6.

Yueh TY, Chen YY, Hwang CL (2006). Properties of HPC with recycled aggregates. *Cement and Concrete research*, 36, 943-950.

Zega CJ, Di Maio AA (2003). Recycled concrete made with different natural coarse aggregates exposed to high temperature. *Construction and Building Materials*, 23, 2047–2052.

Challenge Journal of Structural Mechanics

Research Article

Structural analysis of reinforced concrete mansard roof structures according to different structural plans

H. Selim Şengel [a,*], İsmail Kanber [b], Serdar Çarbaş [c]

[a] *Department of Civil Engineering, Eskişehir Osmangazi University, 26480 Eskişehir, Turkey*
[b] *Graduate School of Natural and Applied Sciences, Eskişehir Osmangazi University, 26480 Eskişehir, Turkey*
[c] *Department of Civil Engineering, Karamanoğlu Mehmetbey University, 70100 Karaman, Turkey*

ABSTRACT

In this study, analysis and evaluations were carried in order to determine the optimum conditions of reinforced concrete mansard roof applications. In total 96 mansard and 24 non mansard structure analysis were performed. The constructed models are symmetrical from all directions and it is modeled under the minimum conditions allowed by the regulation. As the column span, the distance between the columns was determined as 4 meters. The span conditions were determined as 3 spans, 4 spans, 5 spans and 6 spans by evaluating the parcel sizes and zoning conditions. Thus, a total of 120 calculation models were created. The base shear force, column moments and the maximum top displacement values were discussed in concordance with these calculations. As a result of the analysis, the graphical values of the mansard buildings were examined along with the non mansard buildings from the 3rd floor to the 8th floor, according to the zoning plan. In this study, graphs of parcels, span values and the number of storeys were drawn by keeping the values constant, and evaluations were made on the same graphs with and non mansard. In addition, by looking at the movements of the graphs obtained from this study on the same series, equations were adapted to the graphs and the series created with these equations were expanded and stochastic parabolic cones were formed at the shear force for 10 storeys, in the column moments. The mean values for the top displacement chart were taken and when the 20-storey displacement value was placed on this curve, it was determined that it appeared at a point very close to the estimating equation curve. Based on the analysis results, it is understood that it is possible to create a set of estimations for different number of storeys and plans.

ARTICLE INFO

Article history:
Received 27 March 2019
Revised 16 May 2019
Accepted 22 May 2019

Keywords:
Mansard roof
Reinforced concrete
Span
Estimate
Displacement

1. Introduction

Mansard roof is often applied to facilitate the use of the inter-roof without increasing the number of storeys. Roofs in Turkey generally are discarded, unused spaces. Mansard roof, however, provides an aesthetic form for these idle areas and creates areas of use (Üstün and Kolsal, 2016). Mansard roofs are constructed using wood and steel all around the world, however since 2014, an intensive reinforced concrete mansard roof application has been carried out in Eskişehir.

In this study, mansard roof reinforced concrete buildings located inside the provincial border of Eskişehir were examined in accordance with the license information and it was determined that mansards in the region were mostly 3 storeys, 4 storeys, 5 storeys, 6 storeys, 7 storeys, 8 storeys, buildings. When the Urban Development Plan of Eskişehir province was examined, it was determined that there were 3 different parcel types in use. These are adjacent parcels, corner parcels and discrete parcels.

According to the license data in Eskişehir province, 77% of the buildings in 2017 were manufactured as reinforced concrete. The applications of Mansard roofs in Eskişehir are 95% reinforced concrete and 5% of them are constructed as steel. In this study, the most appropriate solutions for mansard roof are investigated and the data obtained from mansard roof solution results are aimed to create prediction model graphs. While creating these models, storey change and mold plans were created. 4 meters between the axes were preferred in order to produce suitable spaces from the specified pattern plans. The pattern plans are composed of 3, 4, 5 and 6

* *Corresponding author*. Tel.: +90-222-239-3750 ; Fax: +90-222-229-0535 ; E-mail address: ssengel@ogu.edu.tr (H. S. Şengel)
ISSN: 2149-8024 / DOI: https://doi.org/10.20528/cjsmec.2019.02.003

spans, respectively. In this study, the entire mansard roof and structural material were preferred as reinforced concrete material. The variables determined in the model are the type of parcels, the number of storeys, the number of spans in the mold plan, and in this way, a total of 96 mansard and 24 non mansard model analysis were created.

In this study, the mansard roof application information in Eskişehir was investigated and the types and models of the structures to be analyzed were determined. Then, for these analysis models, the license details of the existing projects have been taken into consideration. While determining the sections and dimensions in the plans, TS-500 (2000), TS-498 (1997) and DBYBHY (2007) controls were made by using IdeCAD (2014), and analyses of the selected sections of mold patterns were made in SAP2000 (2016). From here, the base shear forces, shear values and moment values formed under the mansard layer were obtained. The graphs of these values were drawn and the interpretation of the graphs were used to investigate the behavior of the mansard roof plans at different parcels types, different spans and storey heights, along with appropriate value conditions. These results were evaluated together with the previous analysis results and estimation curves and graphs were created.

These curves and graphs were evaluated together and real solutions and forecasting graphs were overlapped. Thus, light was shed on the future with the prediction values of different storey and span solutions.

2. Materials and Models

According to the information obtained from DBYBHY (2007), Eskişehir province is a province located geographically in the Central Anatolia region and in the Porsuk Basin. Eskişehir due to its location in Porsuk basin, generally has a clayey and silty soil. In general, structuring is concentrated in areas where Z2 and Z3 ground group are located. Eskişehir is classified as a second-degree earthquake region.

Eskişehir's Central Districts are Tepebaşı and Odunpazarı districts. In line with the information received from the provincial municipalities, the number of storeys in the analysis models has been determined as 3, 4, 5, 6, 7 and 8. In addition, analysis models for estimation charts were also drawn for 10 storeys and 20 storeys.

2.1. Schematic representation of Mansard roof structures to be examined in accordance with the parcels in Eskişehir

When the building regulations of the buildings in Eskişehir and the parcels in Eskişehir were examined, it was observed that the parcels of the mansard buildings were mostly disjoint parcels, adjacent parcels and corner parcels (Fig. 1).

2.2. Coding of building models to be analyzed and mold plans

The coding of the structural models for 120 analysis in the study was preferred for the convenience of naming graphics drawings, charts and processes. While coding, each account model was given names and it was aimed to archive the accounts while trying to make it easier to read and record the data (Kanber, 2018).

In coding, the first digit is arranged to indicate the number of storeys, the next digit is span, and the last digit is Parcel. 3-span models have 3 X-direction spans and 3 Y-direction spans. The distance between each span is 4 meters. Pattern plans are symmetrical in X and Y terms, thus preventing torsion irregularities. The minimum sections were determined using IdeCAD (2014) prior to entering data into SAP2000 software. The columns are 40x40 cm, the beams are 25x36 cm and the slabs are 12 cm. In Fig. 2, mold plans are given for 3 spans, 4 spans, 5 spans and 6 spans.

The soil class was determined as Z3 since it is a common ground class in Eskişehir, and it was taken as T_a=0,15 s, T_b=0,6 s. Z3 elastic acceleration spectrum of the local soil class used in the analysis, special design acceleration spectrum according to DBYBHY (2007) was used. Characteristic compressive strength of concrete was assumed as 25MPa, Modulus of elasticity is 30000 MPa. The coefficient of thermal expansion is 0.00001, Poisson's ratio is 0.2. S420 grade reinforcement is selected as longitudinal and winding reinforcement. The characteristic strength of the equipment was taken as 420 MPa. Elasticity module has been taken as 200000 MPa and tensile strength as 500 MPa.

Fig. 1. Representation of disjoint parcels, adjacent parcels and corner parcels.

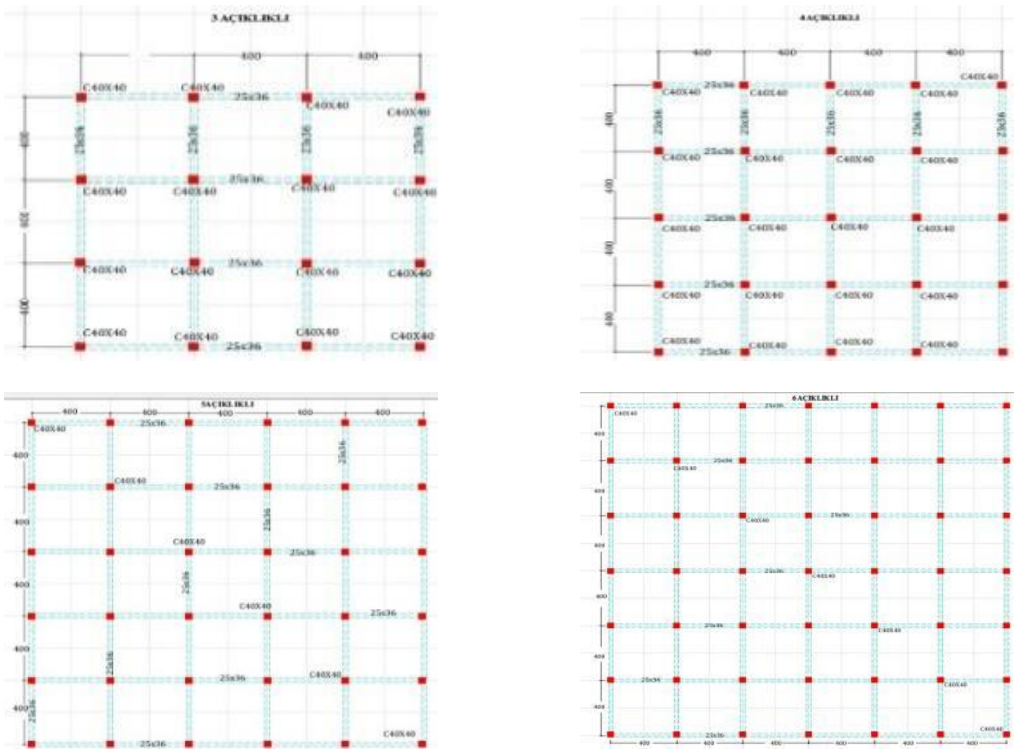

Fig. 2. Schematic representation of the pattern plan for 3 spans , 4 spans, 5 spans and 6 spans.

3. Analysis Results

3.1. The results of the analysis obtained when the parcel is constant, the number of storeys and the openings are variable, and it's evaluation

The change between the values was observed by keeping the parcel option fixed. Thus, the effects of the parcel condition on a reinforced concrete structure were investigated. 12 analysis were performed for each 3, 4, 5, 6, 7 and 8-storey models. In this way, model analysis group with mansard accounts to 72 units. As a result of the analysis; 3 span corner parcel moments are more than 66% adjacent and more than disjoint parcels. 4 span corner parcel moments are more than 53% adjacent and more than disjoint parcels. 5 span corner parcel moments are more than 53% adjacent and more than disjoint parcels. 3 span corner parcel moments are more than 36% adjacent and more than disjoint parcels.

3.1.1. Vertical forces graph created by keeping the parcel option constant

Graphic movements have been examined as the vertical force graphs were evaluated and the parcel status remained constant. The effect of the openness on the vertical force was studied by evaluating the vertical forces together with the series.

When the Fig. 3 is examined, the vertical forces of the base shear force the 6 span are increased for the disjoint parcels. The graphics for the mansard and the non structure are provided together.

It was observed that the proportional increases in Fig. 3 were also very close to the adjacent and disjoint parcels.

3.1.2. Base shear force graph created by holding the parcel option fixed

In this section, the base shear forces are graphically drawn and evaluated. When drawing graphs, series were created, these series were created for 3 span, 4 span, 5 span and 6 span.

The change in shear force in Fig. 4 was obtained by fixing the parcel type in the corner parcel. The base shear forces of the corner Parcel are very close to the adjacent and disjoint parcel.

3.1.3. Moment graph created by keeping the parcel option fixed

In this section, parcel option is fixed and series are created, graphics are defined. While creating these series, groups for 3 span, 4 span, 5 span and 6 spans were formed and these groups were discussed in the same graphs.

In Fig. 5, column moments are given together with the change of aperture on the corner parcel. This change increases with the increase in openness and the increase in the number of storeys.

Considering the column moment of Mansard and non mansard structures; With a mansard roof structure, the moments of a 3-storey and 3-span structure are close together, with the increase in the number of spans and storey, and the difference between the column moments of Mansard and non mansard structures increases. It is observed that the main factor in this difference is not increase in the storeys but increase in the openness.

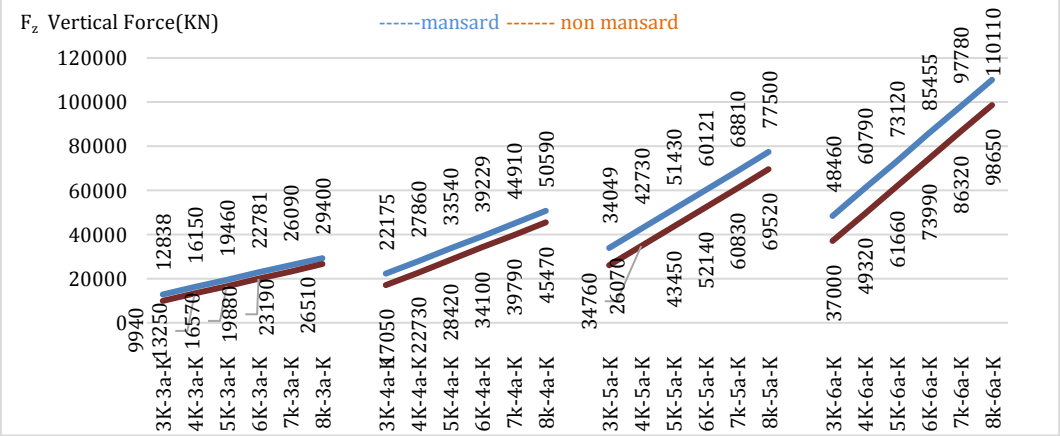

Fig. 3. Vertical forces of columns for the corner parcel when the parcel option is fixed.

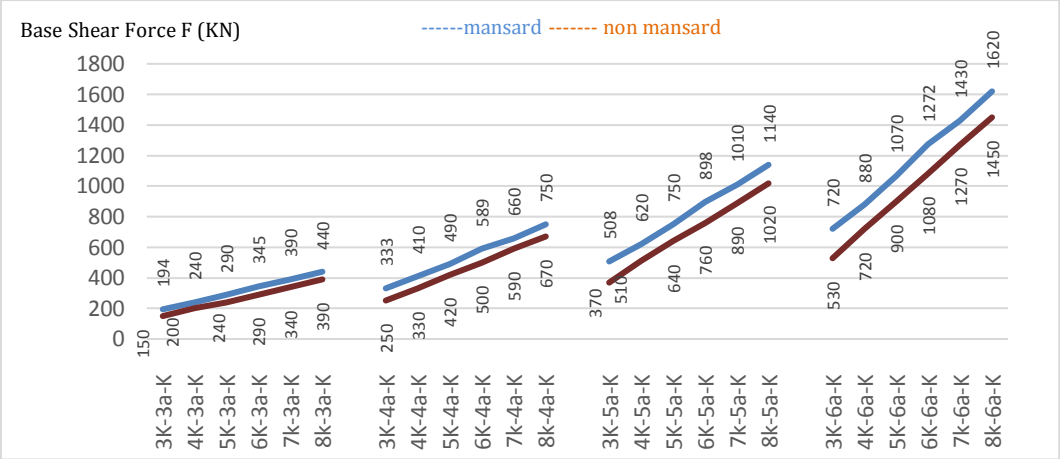

Fig. 4. Base shear forces of F columns for the corner parcel when the parcel option is fixed.

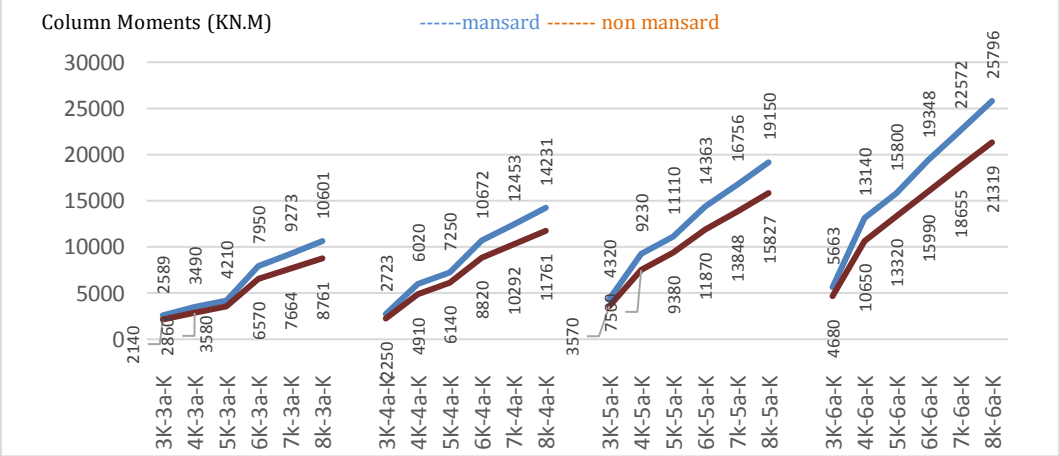

Fig. 5. Graph of column moments for corner parcel when parcel option is held constant.

3.2. Analysis results and evaluations when the numbers of storeys, fixed parcels and openness are variable

When the number of parcels and the number of spans (3, 4, 5, 6, 7 and 8 storeys) of the building with mansard roof are variable, the values obtained as the result of the analysis are obtained as base shear forces, column moments and top displacement.

3.2.1. Vertical forces formed by keeping the number of storeys constant

Vertical force graphs are listed below when the storey quantity is kept constant. For the vertical forces, the forces of the mansard and non mansard structures are given together. Force differences between mansard and non mansard structures are increasing with increasing openness.

When keeping the storey quantity constant for 5 storeys, the graphs were drawn so that the values of the adjacent and corner parcel were examined.

As shown in Fig. 6, in a 5-storey structure, the number of storeys and the fixed opening value were determined as variables in the same graph. Looking at these variables, 3 span, 4 span, 5 span and 6 spans appear together.

The proportional increases observed in Fig. 6 were also found for 3 storeys, 4 storeys, 5 storeys, 7 storeys and 8 storeys.

These graphs which are formed by keeping the storey quantity constant shows us that the effect of parcel type change on vertical forces is low. In addition, it is understood that the situation does not change with the increase in the number of storeys and although the number of storeys changes, this increase is similar to each storey.

3.2.2. Shear force graph created by keeping the number of storeys constant

In Fig. 7, the shear force is not affected by the change in the parcels, although the shear force increases with the increase in the openness.

In Fig. 7, the shear force of mansard and non mansard structures are parallel to the horizontal axis and this shows that the shear force is not affected by the parcel condition. The difference in shear force between mansard and non mansard buildings is also increasing in case of increase in openness for 6 storeys. The same proportional increases were found for 3 storeys, 4 storeys, 6 storeys, 7 storeys and 8 storeys.

3.2.3. Graph of moment forces generated by keeping the number of storeys constant

In this section, the storey number is fixed and the series is formed for 3 span, 4 span, 5 span and 6 spans on the chart. These series are evaluated together. Thus, the effect of the parcel type on the structure is intended for evaluation.

In Fig. 8, the number of storeys for 5 storeys was fixed and the graphics of the structures with and without Mansard were drawn together. Although the structure with mansard and the structure without Mansard increase in openness, the change of the parcel did not affect the moment values.

When we look at the moment graphs created by keeping the storey quantity constant, it is determined that the moment values for the same storey are independent of the parcel condition. When the moment values are evaluated together for mansard and non mansard structures, the difference in the two structure values is increasing in the column moments formed at the base with the increase in the openness in these graphs.

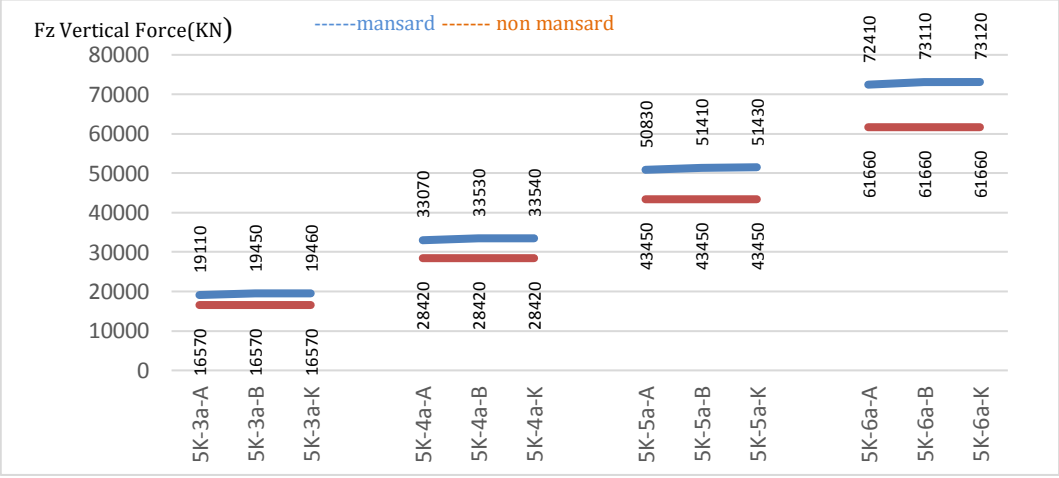

Fig. 6. Vertical force graph created by keeping the storey quantity constant for 5 storeys.

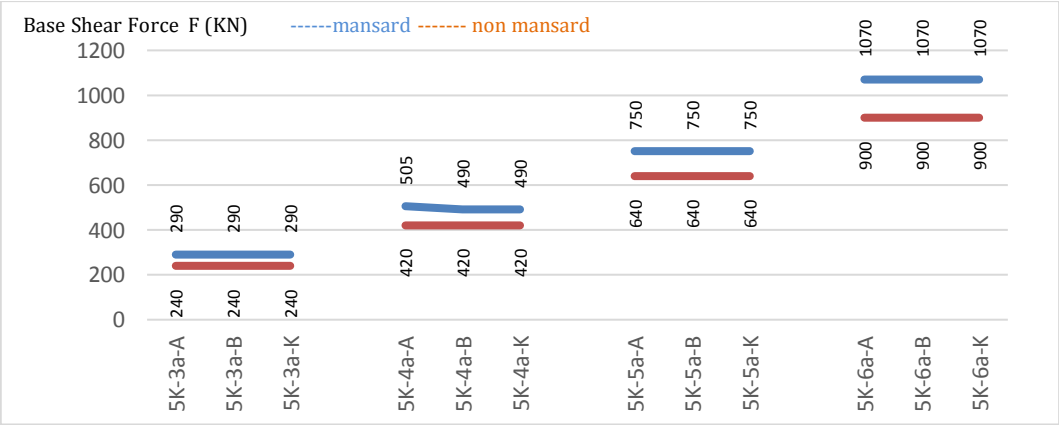

Fig. 7. Base shear force graph created by keeping the storey quantity fixed for 5 storeys.

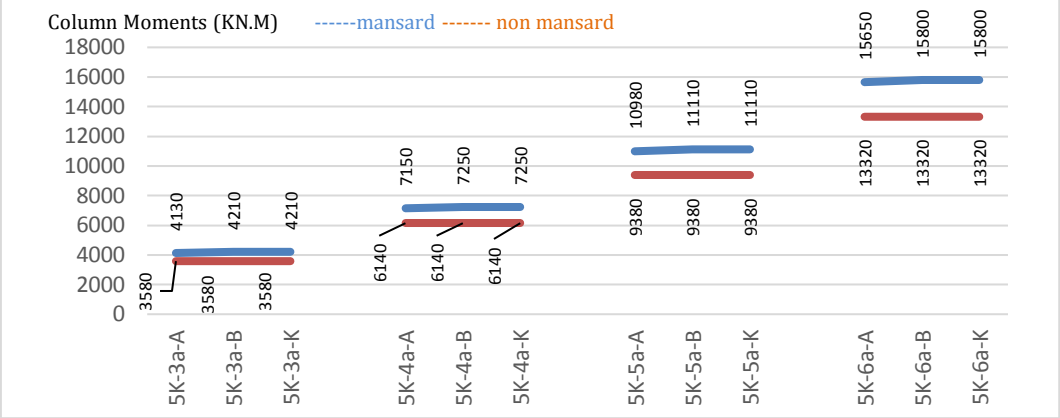

Fig. 8. Moment graph created by keeping the storey quantity constant for 5 storeys.

3.3. Analysis results and evaluation when the openness is constant, the number of storeys and the parcel option is variable

It is aimed to see effect values by keeping openness constant. The parcel option and the number of layers were variable when the spans was kept constant. When the number of spans with mansard roof is fixed, parcel and storey quantity is variable, the values of the base shear forces, column moments and top displacement obtained as a result of analysis are examined. Graphs are drawn for base shear force, column moments and top displacement values.

3.3.1. Vertical forces graph when the aperture is held constant

The effect of vertical forces was observed by keeping the aperture constant. The increase in the number of storeys increases the vertical forces. The parcel variable does not affect the vertical forces very much when looking at the adjacent parcel and the corner parcel from the disjoint parcel.

In Fig. 9, the vertical forces given for 5 openings show a linear increase. The increment slopes of the disjoint parcel, adjacent parcel and corner parcels are the same. The same proportional results were found in 3 spans, 4 spans and 6 spans. When the angle is fixed, it is observed that the motion of the shear force is linear from 3rd to 8th storey. While the shear force increases linearly from 3rd storey to 6th storey, the curvature angle of this linear graph is very little affected by the change in the parcel change.

3.3.2. Graph of shear forces when the span is held constant

Fig. 10 shows a linear increase of the base shear forces given for 5 spans. The increment slopes of the disjoint parcel, adjacent parcel and corner parcels are the same. Mansard and non mansard buildings are provided together. The slope in the shear graph of Mansard and non mansard is the same. The same proportional results were found in 3 spans, 4 spans and 6 spans.

3.3.3. Moment graph when opening is fixed

In Fig. 11, moment values were taken by keeping the openness constant, and it was observed that the parcel variable was not affected when evaluating the 5 openness in different parcels. The same proportional results were found for 3 spans, 4 spans and 6 spans.

When the span is held constant moment graph shows increase from the 3rd storey to the 8th storey. When looked at the parcel change, disjoint, adjacent and corner parcels show a very close moment change ratio. The difference between the moment values of mansard and non mansard structures are increasing as we move from 3 spans to 6 spans.

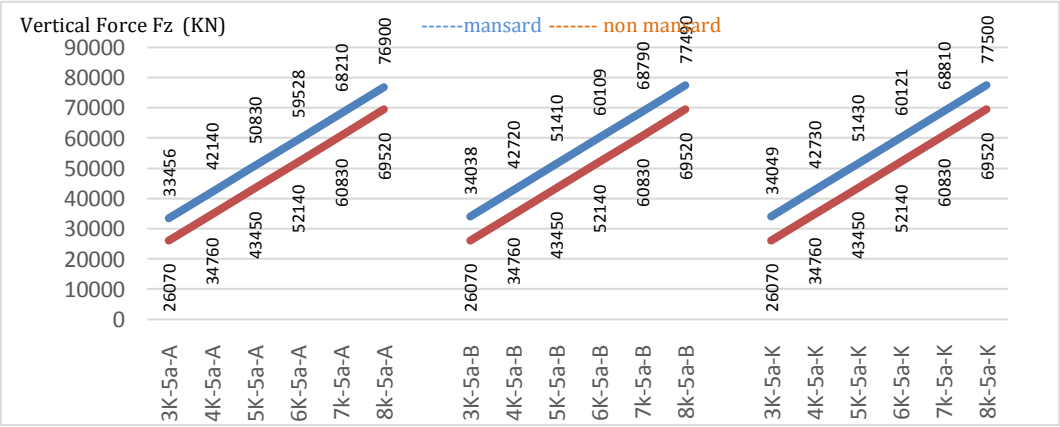

Fig. 9. Vertical force graph created by keeping the openness constant for 5 spans.

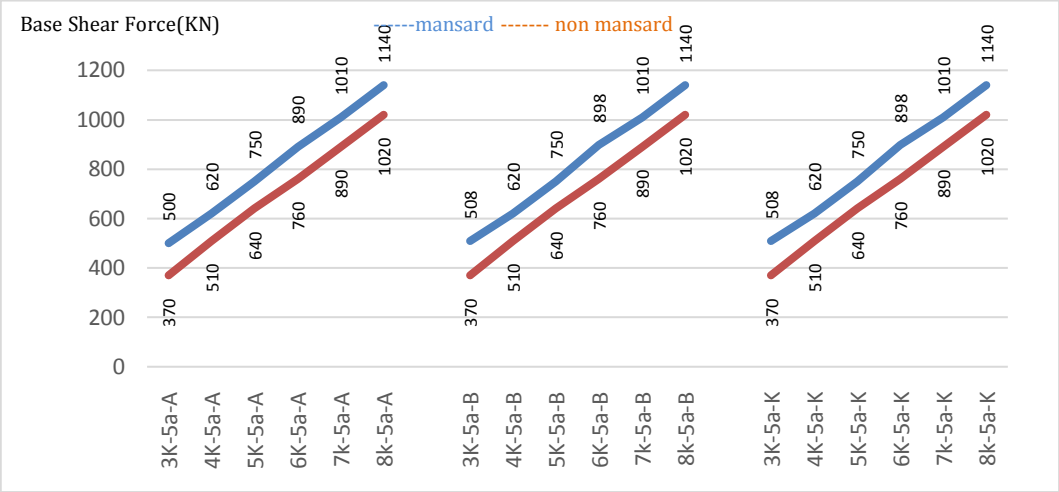

Fig. 10. The base shear force graph created by keeping the span constant for 5 spans.

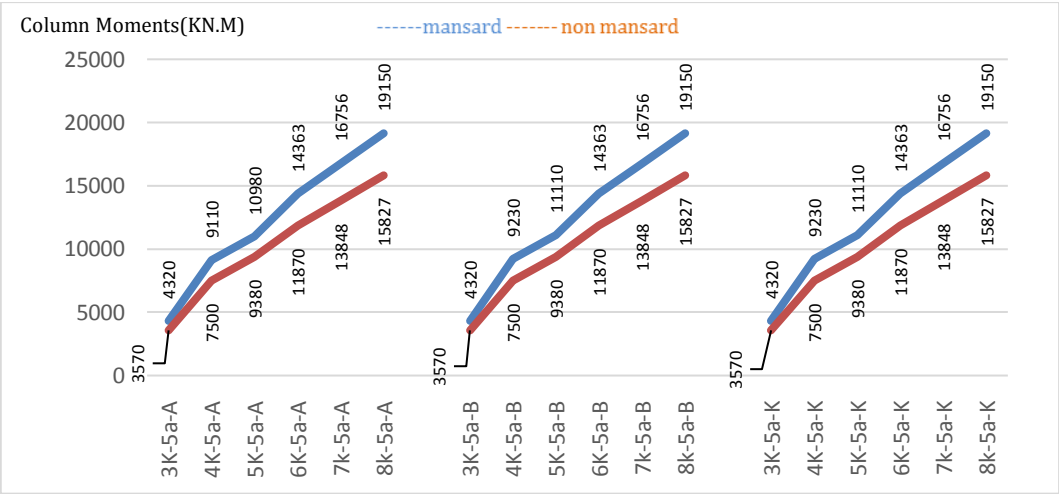

Fig. 11. Moment graph generated by keeping the span constant for 5 spans.

3.4. Creating forecasting functions

Based on the results obtained from these analyses, graphs were drawn for each set of results, and most appropriate mathematical functions were obtained from these graphs. How close these functions are to reality is also verified by comparing the solutions of intermediate values (such as storey counts. etc.). Thus, a forecast projection of the base cut and moment values has been created depending on the openings and parcel variables from 3rd storey to 10th storey.

Firstly, the parcel variable is fixed and the graphics are defined. Parabolic graphs are placed on the graphs formed according to these definitions. The reason for the formation of parabolic charts and the formation of graphs is the form of increasing graphics curves.

A new graphic definition has been created by combining the solution series and is tried to understand the relation between this graphic definition and the solution series.

In Fig. 12, a parabolic chart was used for trying to capture the motion of the variables in the following units, and these values were moved on the X axis within them.

These values are shifted in line with the X axis, giving a parabolic graph and shown in Fig. 13. In Fig. 12, parabolic graph of reinforced concrete mansard roof and non mansard roof is given, and in Fig. 13, the graph of mansard roofed structure group is given. In Fig. 12, parabolic graph inside the F force is examined for the non mansard reinforced concrete structure. Figs. 12 and 13 show a parabolic graph and it is understood that equations can be obtained from these graphs.

As shown in Fig. 14, the given values are defined as parabolic equation by matching with some values in the series. The values in this graph are determined by the actual results obtained from the analysis. Fig. 13 shows us that these graphs can be connected to specific formulas in the series formation. It is understood that new graphs can give prediction values for new series.

In Fig. 15, the data obtained by using the analysis program of the 10-storey building was found to be in the mobile wave area.

If this series is expanded and replicated by this quality, it will multiply in the same quality as the parabolic cone. Due to this proliferation, it will be expected that the values in different storey and span structures will remain between these ranges. When the integral of these functions is taken, value interval estimation can be made within the new series that will be formed.

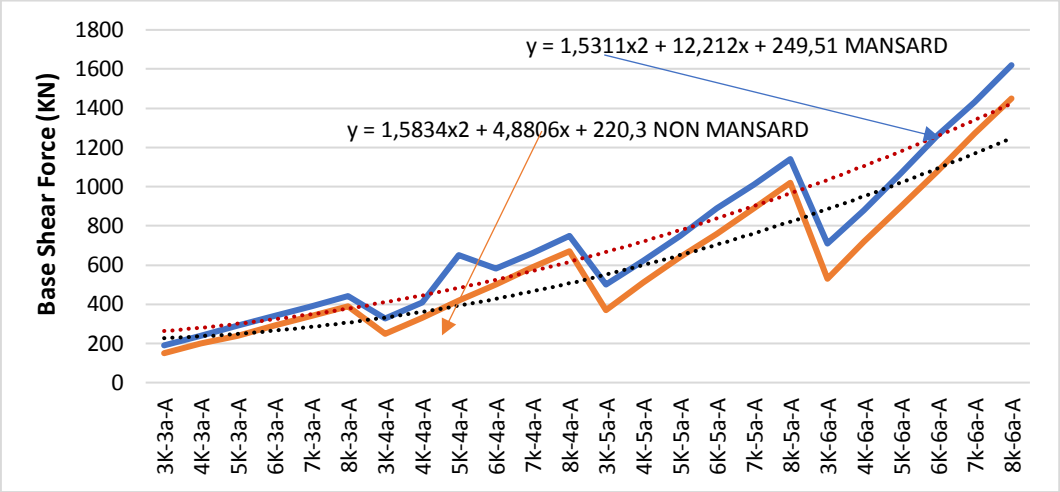

Fig. 12. Parabola placement on drawn graphics.

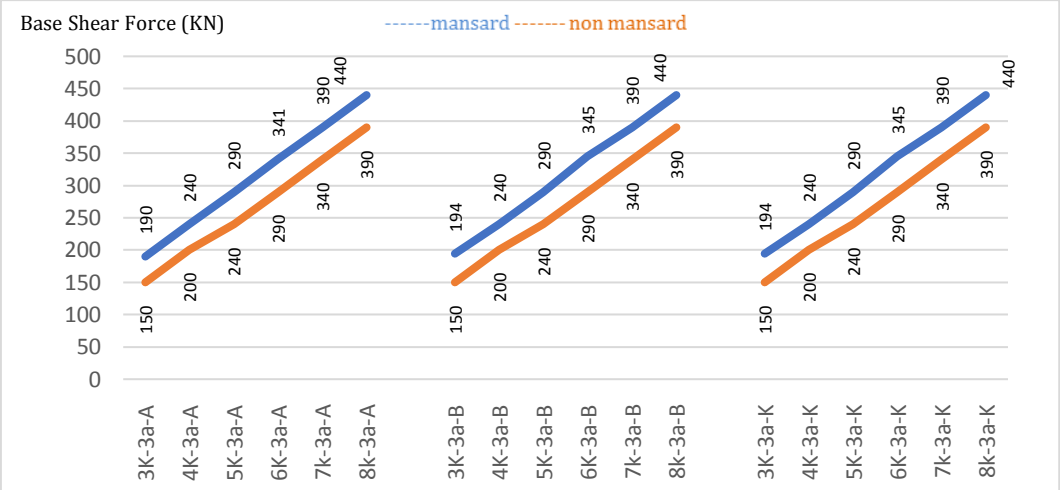

Fig. 13. Analysis of base shear force graph as series.

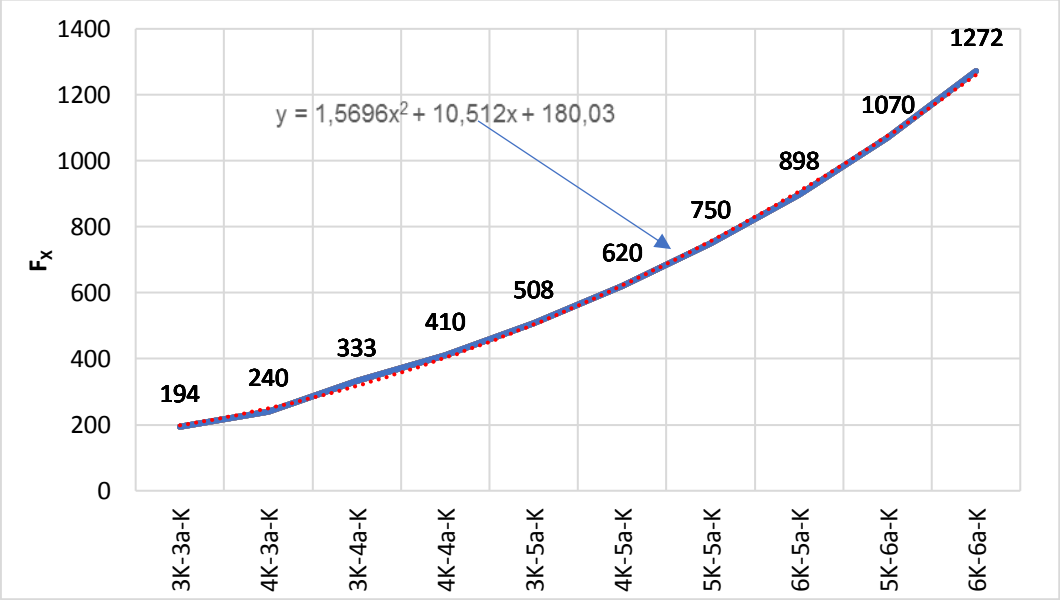

Fig. 14. Defining a parabolic rectifier for force *F*.

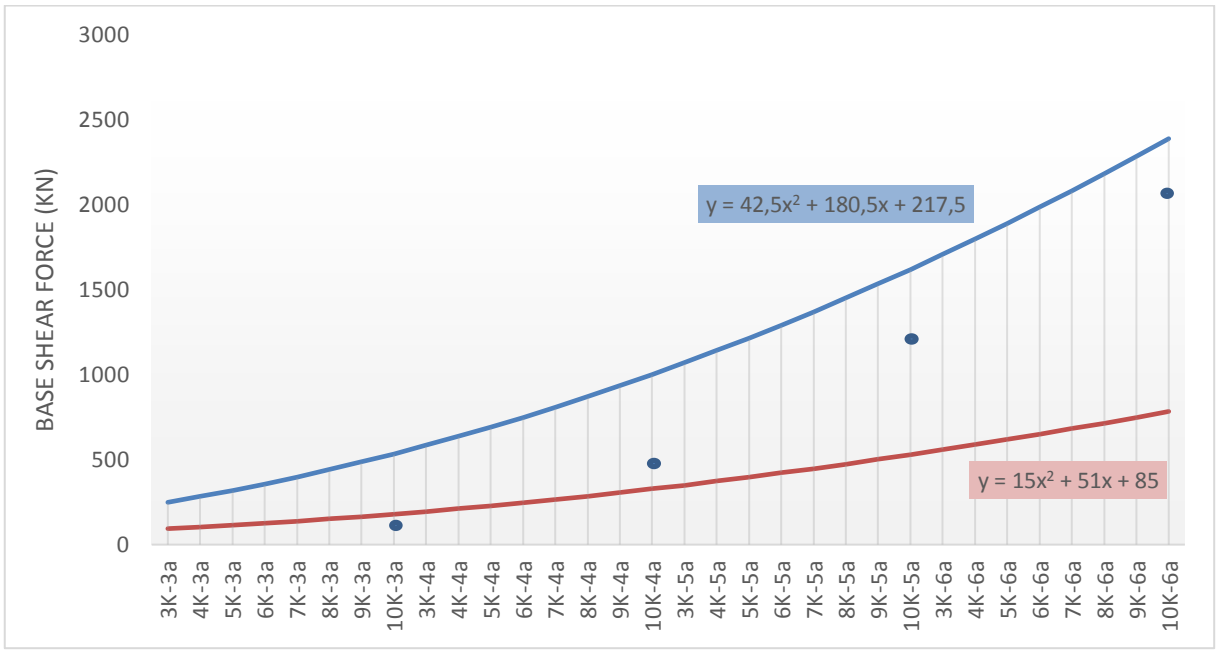

Fig. 15. 32 Piece 3rd to 10th storey estimated series graphical drawing.

The determination of these prediction functions for the shear force is also done for the moments and the values of the analysis are processed in the series on the chart. The moment values of the 10-storey reinforced concrete structure remain within this graph range as shown in Fig. 16. Therefore, in this series consisting of 3 storeys to 10 storeys, 3 spans to 6 spans and the parcel can be estimated value range depending on the situation.

A curve was drawn to the average displacement values and the displacement values of the 20-storey structure were added on this curve. In this way, it is seen how close the real values of the 20-story structure are to the prediction curve. The equation graph was drawn in line with the results obtained from the average displacement values and a 20-storey structure of series was added to the sub-axis on this equation. Thus, a prediction curve has been formed for the displacement values of the structures up to 20 storeys. It was observed that this value was very close when structural analysis for 20 storey buildings was added to the prediction curve. The graphs created together with the set of values from here shed light on the prediction of new values. Thus, it has been revealed that the other displacement values remaining within the range can be estimated using Fig. 17 chart.

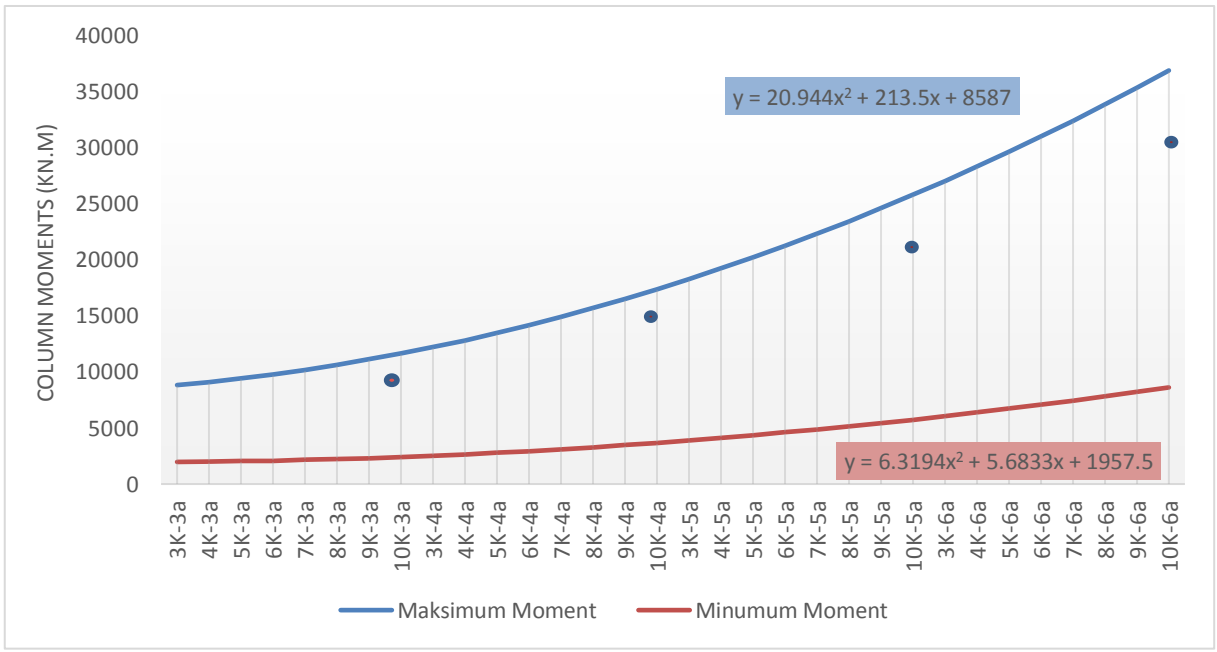

Fig. 16. 32 Piece graphical drawing from 3rd storey to 10th storey.

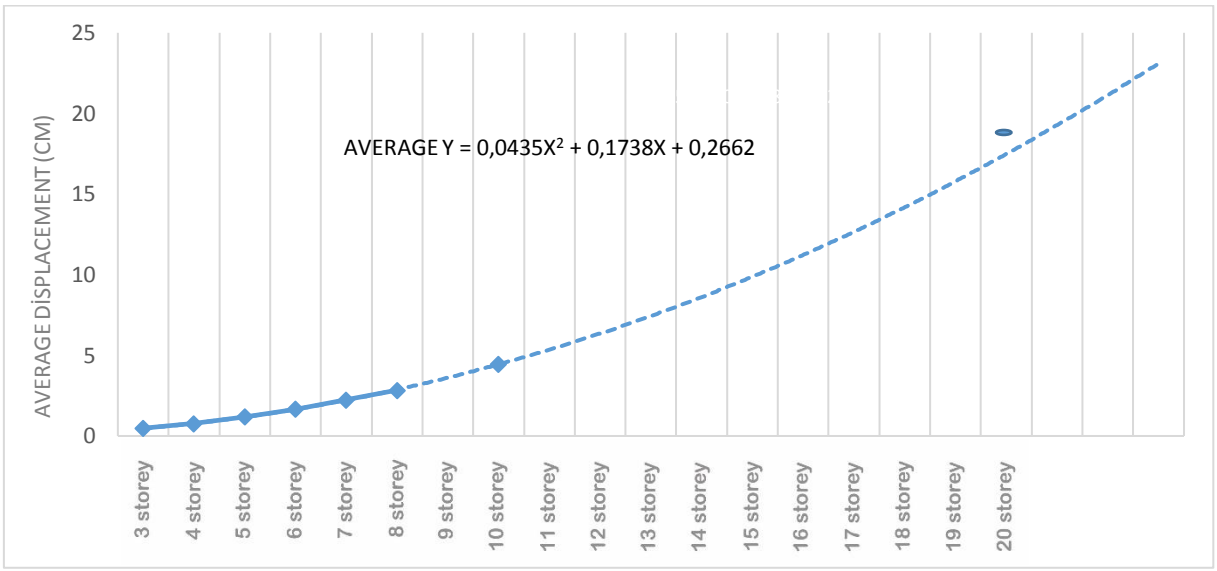

Fig. 17. Average displacement graph.

4. Conclusions

In this study, 96 mansard and 24 non mansard model analyzes were performed for the reinforced concrete structure. Values from these structures up to 3 to 8 storeys and from 3 openings to 6 openings were defined and analyzed in the light of Eskişehir license information and their results were evaluated. As a result of these evaluations, the increase in storey and openness increases the increase in parabolic base shear and column moment increases on the structure. As a result of the investigations, it was observed that the displacement values were very close to each other when the effects of displacement values on the same storey buildings were examined. This shows that the value of displacement is too small to be taken into account. In this study, it is understood that displacement values are independent of openness.

As a result of the analyses obtained from models with different spans and storeys, base shear force, column moments and top displacement values were evaluated in charts and graphs. It is estimated that the function we obtain depends on the set of values of these series can be obtained by the user, depending on the prediction projection, without making any analyses based on the different number of layers. Functions have been created and equations have been written in defined series. These functions are created for base shear force, column moments and top displacement values. New series are defined and graphs are drawn in accordance with these new series. 10-story and 20-story buildings, 3 spans to 6 spans were analyzed and the new series were added as a point value to the graphs of the defined series. Based on the results of the analysis, it was determined that the function graphs created for estimation remained within the range. The graphics and the functions that will be obtained from the range that is defined as series are able to create a prediction interval about the base shear force, colon moments and peak displacement values of the models that will sustain the mentioned series, which have different openness' and storey counts.

Analysis results can be defined by graphs and functions with the minimum and maximum values of the base shear forces and moments listed by series. Thus, the estimation range for different storeys and openings was defined and the estimation projection was determined by the expansion of the series in the solutions of the defined equations.

Equations are formed by the results obtained from the average displacement values. Since displacement is not affected by openness, an estimate of the values to be formed on different storeys was carried out with a single prediction equation.

In this study, symmetric models are used, it is recommended to analyze non-symmetric systems in future studies and so an approach for all symmetric and non-symmetric systems can be developed. In addition, this study can be done by increasing the number of solutions and analyzes in the set of values and increasing the sensitivity for estimation graphs.

References

DBYBHY (2007). Regulation on Buildings to be held in Earthquake Areas. General Directorate of Disaster Affairs, Earthquake Research Department, Istanbul, Turkey.

IdeCAD (2014). Concrete Analysis Program. Version ideCAD 7,022, 6500HL-3109 Static.

Kanber İ (2018). Analysis of Reinforced Concrete Mansards Roof Structures Dependent on Different Plan Types. *M.Sc. thesis,* Eskişehir Osmangazi University, Eskişehir, Turkey.

SAP2000 (2016). Finite Element Analysis Program. Version SAP2000 v 17.2.0.

TS–498 (1997). Calculation of Loads to be taken for Sizing of Building Elements Values. Turkish Standards Institute, Ankara, Turkey.

TS–500 (2000). Design and Construction Rules of Reinforced Concrete Structures. Turkish Standards Institute, Ankara, Turkey.

Üstün B, Kolsal F (2016). Mansard roof in Eskisehir urban architecture effects. *8. National Roofing & Facade Symposium*. Mimar Sinan Fine Arts University, Istanbul, Turkey, 1-7.

Challenge Journal of Structural Mechanics

Research Article

Arch effect in silos on discrete supports - Is it a myth or reality?

Lyubomir A. Zdravkov *

Department of Metal, Wood and Plastic Structures, University of Architecture, Civil Engineering and Geodesy (UACEG), Sofia 1046, Bulgaria

ABSTRACT

Steel silos are interesting, complicated facilities. In order to assure its complete emptying by gravity they are often placed on supporting frame structure above the ground. Values of stresses in joints between thin walled shell and supporting frame elements are very high. It can cause the local buckling in the shell. The simplest way to design steel silos is to divide hypothetically the cylindrical shell into two parts - ring beam, supported in some points and shell above, uniformly supported. This conception is accepted by European Standard EN 1993-4-1. The particular moment is that the ring beam and cylindrical body above it are separated. Actually the two elements are jointed and work together in the same time. Considering the last results of Zeybek, Topkaya and Rotter from 2019, and as well as his own research, the author asks the question if it is true that the transferring of discrete base reactions to the cylindrical body is done by bending work of the ring beam, which is the conception in EN 1993-4-1? Or the vertical reaction forces are actually redistributed on the height based on the work of the cylindrical shell under compression as an arch. Using the contemporary capabilities of the programs for spatial analysis of building structures the author will try to find the answer of this question.

ARTICLE INFO

Article history:
Received 10 March 2019
Revised 3 May 2019
Accepted 8 June 2019

Keywords:
Steel silo
Meridional stress
Ring beam
Arch effect
Vertical stiffening
Buckling

1. Introduction

Usually the steel silos are elevated above the ground facilities, placed on supporting structure. The purpose is to assure the easy and complete emptying of the stored product by gravity. The supporting structure is different for every facility because it depends on the real conditions of exploitation. The most used are the two types - built by horizontal girders and columns or only by columns. Both type of frame structures cause concentrated meridional forces in the cylindrical body of the silo. As a result the thin wall shell could buckles.

The simplest way to design steel silos is to divide hypothetically the cylindrical shell into two parts - discretely supported ring beam and uniformly supported shell above it, see Fig. 1. This conception is accepted by the European standard EN 1993-4-1. Obviously, to assure uniform supporting on the whole circumference of the circular shell, bending stiffness of the ring beam should be high. Unfortunately the EN 1993-4-1 does not say what should be the recommended stiffness of the ring beam.

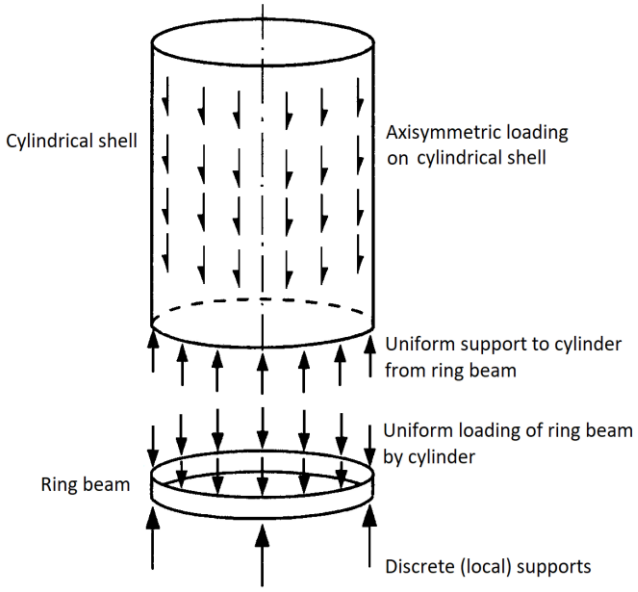

Fig. 1. Traditional design model for silos on discrete supports.

* *Corresponding author*. Tel.: +359-885-081-305 ; E-mail address: zdravkov_fce@uacg.bg (L. A. Zdravkov)
ISSN: 2149-8024 / DOI: https://doi.org/10.20528/cjsmec.2019.02.004

Rotter (1985) suggested that a value of ratio ψ = 0.25 might be suitable for adoption in design, where:

$$\psi = \frac{K_{\text{shell}}}{K_{\text{ring}}} \tag{1}$$

in which:
K_{shell} is stiffness of cylindrical shell;
K_{ring} is stiffness of ring beam.

Based on English translation of study of Vlasov (1961) about of curved beams, stiffness of ring beam K_{ring} is expressed as:

$$K_{\text{ring}} = \frac{(n^2-1)^2 EI_r}{R^4} \frac{1}{f_r} \tag{2}$$

where:
n is number of uniformly spaced supports;
E is modulus of elasticity;
I_r is moment of inertia about a radial axis;
R is radius of ring beam centroid.

$$f_r = 1 + \frac{EI_r}{n^2 K_T} \tag{3}$$

in which:

$$K_T = GJ + n^2 \frac{EC_w}{R^2} \tag{4}$$

where:
G is shear modulus;
J is torsional constant;
C_w is warping constant for an open sections.

Semi-membrane theory of shells, proposed by Vlasov (1964), gives an expression of stiffness of cylindrical shell, as follow:

$$K_{\text{shell}} = n\sqrt{(n^2-1)} \frac{E}{\sqrt[4]{3}} \left(\frac{t}{R}\right)^{3/2} \frac{1}{f_s} \tag{5}$$

where t is thickness of the cylindrical shell.

$$f_s = \frac{(e^{\eta})^2 - 2e^{\eta}\sin(\eta) - 1}{(e^{\eta})^2 - 2e^{\eta}\cos(\eta) + 1} \tag{6}$$

in which:

$$\eta = \frac{2\pi H}{\mu} \tag{7}$$

where:
H is height of cylindrical shell;
μ is expressed by Calladine (1983) long wave bending half-wavelength:

$$\mu = \frac{2\pi \sqrt[4]{3}}{n\sqrt{(n^2-1)}} \sqrt{\frac{R}{t}} R \tag{8}$$

Based on Eqs. (2) and (5), stiffness ratio ψ will look like as:

$$\psi = \frac{K_{\text{shell}}}{K_{\text{ring}}} = \frac{0.76\,(Rt)^2}{I_r} \sqrt{\frac{R}{t}} \sqrt{\frac{n^2}{(n^2-1)^3}} \frac{f_r}{f_s} \tag{9}$$

For simplification, the Eq. (6) could be represented by two simple relations:

$$f_s = \begin{cases} \frac{\eta}{3}, \text{ when } H \le H_{cr} \\ 1.0, \text{ when } H > H_{cr} \end{cases} \tag{10}$$

where H_{cr} is critical height of cylindrical shell. It could be determined by formula:

$$H_{cr} = \frac{3\sqrt[4]{3}}{n\sqrt{(n^2-1)}} \sqrt{\frac{R}{t}} R \tag{11}$$

H_{cr} represents the height of shell which is effective of redistributing of discrete forces from supports and equalizing of axial normal stresses. When height of shell $H \le H_{\text{cr}}$, entire shell resists axial loads from supports. When $H > H_{\text{cr}}$, only that part between bottom of shell and critical height H_{cr} is effective in redistributing of vertical reactions from discrete columns.

In their researches Topkaya and Rotter (2011a) (2011b) conducted extensive finite element analyses for verification of Rotter's criterion about stiffness of ring beam. With 1,280 separate finite-element analyses (FEA), covering two different types of ring sections, various heights and radii of cylindrical shells, the authors checked validity of suggested by Rotter (1985) ratio ψ = 0.25. On basis of done FEA they concluded, when a stiffness ratio $\psi \le 0.1$, axial stresses will not deviate more than 25% from the uniform support assumption.

Research of Zeybek, Topkaya and Rotter (2019) shows that the equations, based on the theory of Vlasov (1961) for a curved beam provide results with acceptable accuracy when the girder is separated from the cylindrical body. When the ring beam and cylindrical shell are jointed, the received through finite elements analysis values are considerably different from the analytical results in closed form. The differences going high with increase of the thickness of the cylindrical shell.

It should be noted that all above mentioned researches are conducted on the smooth steel shells without vertical stiffeners on them. On other side, common practice in design of steel structures is to place stiffening elements on the point, where are applied concentrated loads. In our case, the vertical stiffeners should be placed above the discrete supports, see Fig. 2.

Fig. 2. Stiffening elements above discrete supports of the shell.

In his research Zdravkov (2017a, 2018) shows that vertical stiffening elements increase the height of the critical zone, where the vertical reactions of discrete supports are redistributed. Considering the last results of Zeybek, Topkaya and Rotter (2019), as well as his own research, the author put the question if it is true that redistributing of the separate reactions of supports is done by the bending of ring beam which is the conception in EN 1993-4-1, see Fig. 1. Or vertical forces in discrete supports are transferred on the height by work of the cylindrical shell above the supports as a compressed arch, see Fig.3.

In this article the author will try to find answer of these questions.

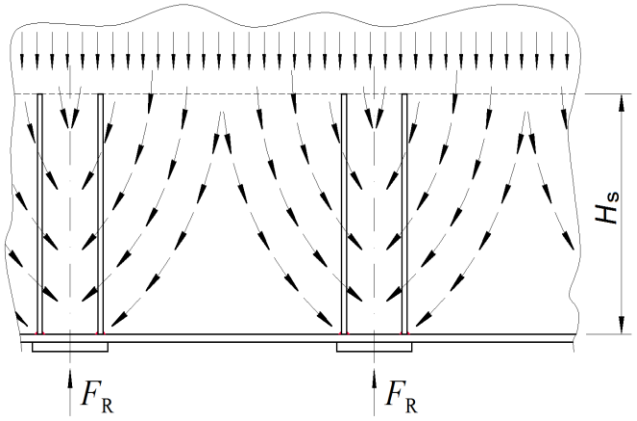

Fig. 3. Compression forces in the cylindrical shells above the supports.

2. Finite Element Analysis

For the purpose of research, three steel cylindrical shells are modelled, using software ANSYS. Their parameters are as follow:

a) Dimensions:
- shell 1 – diameter D = 3 m, height H = 6 m;
- shell 2 – diameter D = 4 m, height H = 8 m;
- shell 3 – diameter D = 5 m, height H = 10m.

b) All shells are with constant thickness t = 5 mm;

c) All shells are supported by six immovable supports with dimensions in plane 125×125 mm, see Fig. 4.

d) In Fig. 4 every support are placed two vertical steel plates with section 8x100 mm and with different height. On their upper end exists an intermediate ring with a section L100x8 mm, see Figs. 4 and 5.

e) Cylindrical body in three models of the shells is continuous, see Fig. 5(a). In the other three models are made openings between the vertical stiffeners, see Fig. 5(b). On this way the "skirt" of the silo cannot works as a ring beam. The support's forces will be transferred up on the cylindrical body only through work of the cylindrical shell above the supports on compression, as an arch, see Fig. 3.

f) The heights of the openings h_o are different, depending on the height of the stiffeners. They are calculated according to the simple formula:

$$h_o = H_s - 100 \text{ mm} \tag{12}$$

where H_s is the height of vertical stiffeners, see Fig. 6.

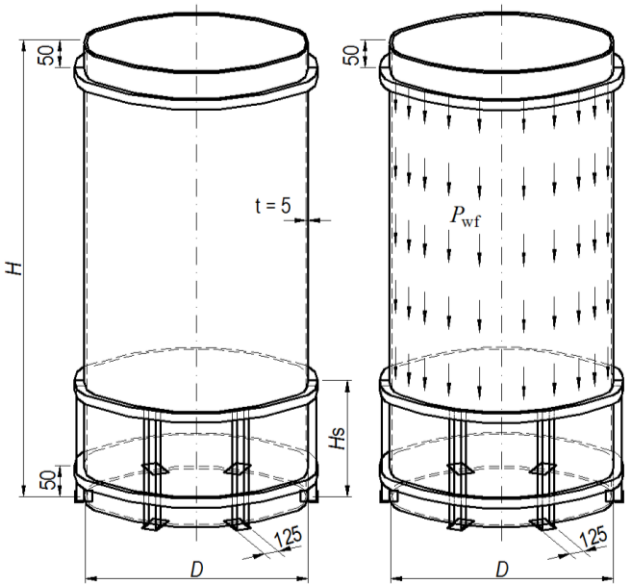

Fig. 4. Numerical models – dimensions and loading.

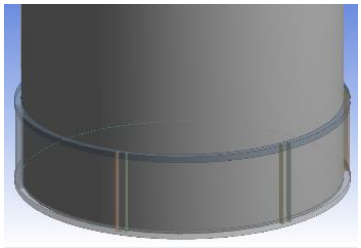

a) shell without opening

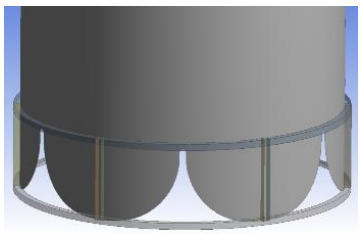

b) shell with openings

Fig. 5. Vertical stiffeners on the cylindrical shell.

g) In order to strengthen the shells in radial direction, on 50mm above the lower edge and on 50mm below the upper edge are placed rings with section L100x8 mm, welded as is shown on Fig. 7.

h) The stored in the facilities product varies. For each shell it is as follow:
- shell 1 – cement;
- shell 2 – lime;
- shell 3 – sand.

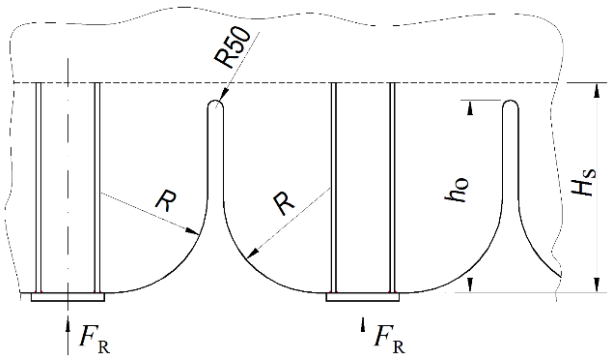

Fig. 6. Opening in the base of the cylindrical shell.

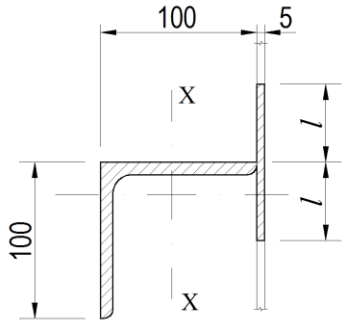

Fig. 7. Shape of the intermediate stiffening ring.

Every product causes vertical load P_{wf} due to the friction between the stored material and the shell. Its values are determined for every particular product according to standard EN 1991-4. All loads are uniformly distributed and applied as a surface pressure on the shell. They are applied to internal surface of the shells, see Fig. 4.

i) Shells 1, 2 and 3 are analysed for four different heights H_s of vertical stiffeners above supports.

The heights reached by the stiffening plates are determined as follows:

- using an average value of distribution of discrete forces F_R from supports $\alpha = 45°$, see Fig. 8. The height H_{45} is determined with the expression:

$$H_{45} = \frac{\pi R}{n} \tag{13}$$

where R is radius of cylindrical shell.

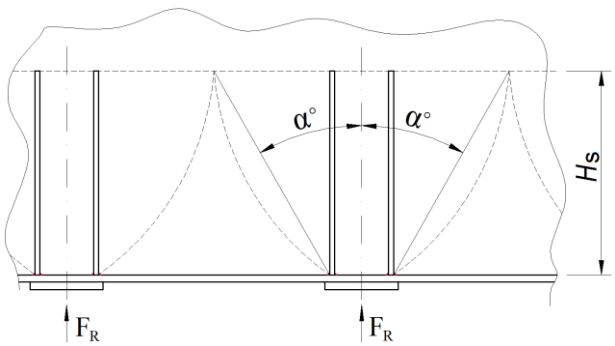

Fig. 8. Average angle α of distribution of the compressive forces on height.

- at ideal position of the intermediate stiffening ring on the shell.

Topkaya and Rotter (2014) determined the ideal position of intermediate stiffening rings on the shell. They expect a ring, placed at this ideal position, can effectively remove all circumferential nonuniformity in the axial membrane stress above it. The simple expression of ideal location H_I is:

$$H_I = \sqrt{12(1+\nu)}\,\frac{R}{n} \tag{14}$$

where ν is a coefficient of *Poisson*.

- using an average value of distribution of discrete forces F_R from supports $\alpha = 30°$. The height H_{30} should be calculated by the formula:

$$H_{30} = \frac{\pi R}{n}\tan(90° - \alpha°) \tag{15}$$

- the length of the stiffeners H_L is equal to distance between the supports. It is calculated according to the formula:

$$H_L = \frac{2\pi R}{n} \tag{16}$$

j) Material of elements is steel S235, with a properties according to European standard EN 10025-2:2004.

Necessary stiffness of intermediate stiffening rings is determined by Zeybek et al. (2015). Stiffness ratio χ could be expressed as:

$$\chi = \frac{K_{\text{shell}}}{K_{\text{stiffener}}} = \frac{Rt\left(AR^2 + I_x n^2\left(n^2-1\right)\right)}{12\sqrt{3}(1+\nu)^{3/2} A I_x n(n^2-1)^2} \tag{17}$$

where:
K_{shell} is circumferential stiffness of the shell;
$K_{\text{stiffener}}$ is circumferential stiffness of circular ring;
A is cross sectional area of the stiffening ring;
I_x is moment of inertia of the stiffening ring about vertical axis "x-x".

The results in research of Zeybek et al. (2015) indicate that ratios below about $\chi < 0.2$ provide a satisfactorily uniform axial membrane stress distribution above the intermediate ring stiffener, so this limit is recommended for practical design. In his later research Zeybek et al. (2017) confirmed, that correlation smaller than $\chi < 0.2$ are sufficient even when the rings are placed under their ideal position.

The steel angle section L100x8 and a part of the cylindrical shell form an intermediate stiffening ring with a shape as is shown on Fig. 7.

Effective width l of the steel sheets over and below the joint is calculated according to the standard API 650, by the expression:

$$l \le 13.4\sqrt{Dt} \tag{18}$$

where:
D is a diameter of the cylindrical shell, m;
t is thickness of the cylindrical shell, mm.

Effective width l for the shells with the smallest diameter, D = 3 m, is l = 51.9 mm. The author accepts to have effective width l = 50 mm for all shells. It is on way of safety.

The geometric characteristics of the obtained stiffening ring are:

a) Area - A = 20.5 cm^2;

b) Moment of inertia about vertical axis „x-x“- I_x=358.4 cm^4.

For different shells, the ratio of the stiffness's χ, calculated according to the Eq. (17), has the values as follow:

- shell 1 – χ = 0.042;
- shell 2 – χ = 0.0764;
- shell 3 – χ = 0.130.

The maximum value of the ratio χ = 0.130 < 0.2, so it could be expected that the stiffness of the intermediate ring will be sufficient to equalize the meridional stresses in the shell above it.

The shells are modeled by 2D quad elements shell181 with a maximum length of side 50 mm. The method of their creation is "All quad". Element's midside nodes are controlled by the program.

Thin shell structures are sensitive for effect of changes of geometry during loading. On that reason geometrically nonlinear analyses (GNA) are used, according to the recommendations of EN 1993-1-6.

ANSYS's option "symmetry" is activated to reduce a calculation time. In analysis is used a quarter of silo only, see Fig. 9.

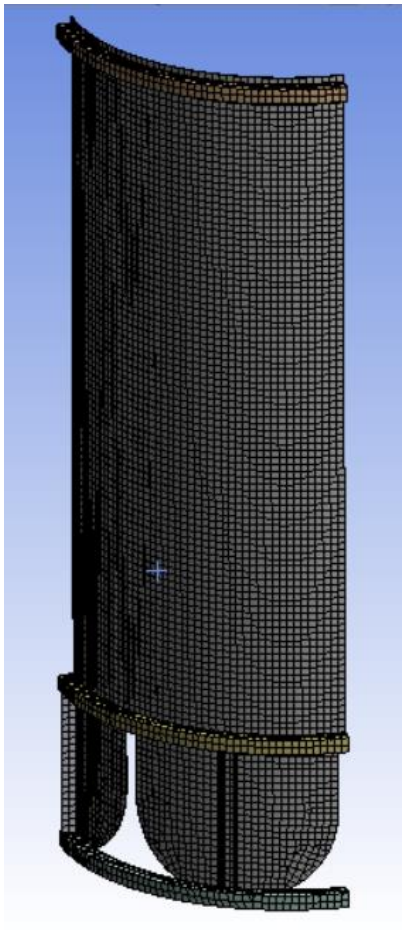

Fig. 9. Quarter of silo, used in numerical analysis.

Axial normal stresses are accounted by the height of shell, in the middle between two supports and above the supports. After that are determined the values of ratio $\sigma_{x,m}/\sigma_{x,s}$, where:

$\sigma_{x,m}$ is meridional normal stress by height of the cylinder, in the middle between two supports;

$\sigma_{x,s}$ is meridional normal stress by height, above the supports.

The idea is that where the ratio $\sigma_{x,m}/\sigma_{x,s}$ =1.0 , is the upper border of the critical zone in the shell, in which are redistributed vertical reactions of supports. Above that border circumferential nonuniformity in the axial membrane stresses does not exists and the shell is continuously supported.

On the second stage, in the used program ANSYS is activated the option "Buckling Analysis". Through this option it is possible to calculate the reserve of bearing capacity k of the cylindrical shell before that it losses stability, completely or partially. The reserve k gives a quantity assessment of the influence of the made openings on the bearing capacity of the shell.

3. Results and Discussion

The graphics below, see Figs. 10-12, show the changes of ratio $\sigma_{x,m}/\sigma_{x,s}$. by height, calculated using numerical methods for analysis.

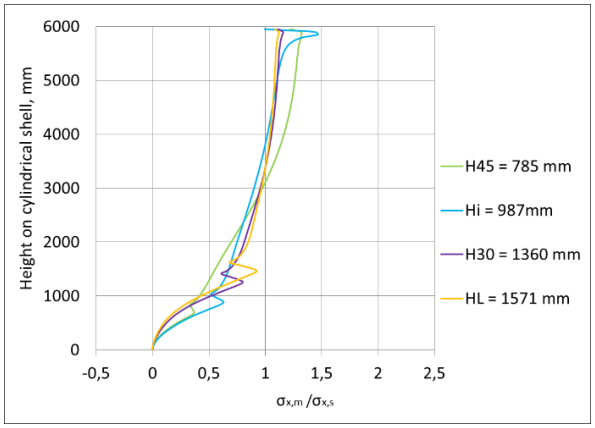

a) without openings in the ring beam

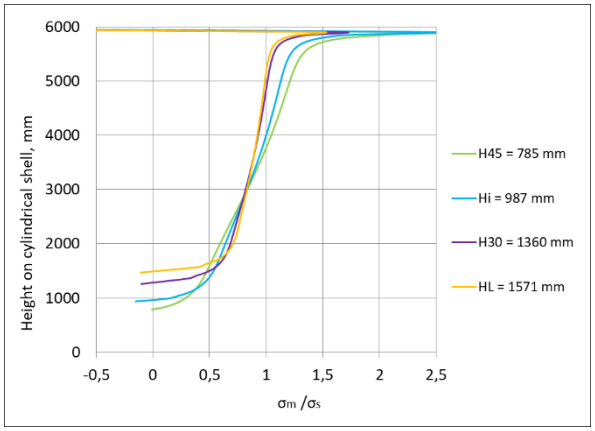

b) with openings in the ring beam

Fig. 10. Change of ratio $\sigma_{x,m}/\sigma_{x,s}$ by the height of the cylindrical shell 1 (D = 3 m, H = 6 m).

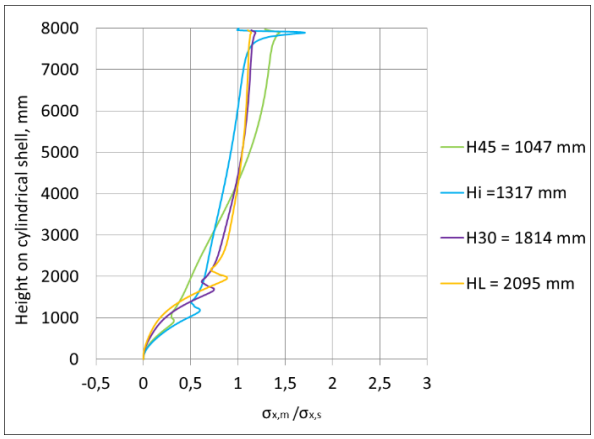

a) without openings in the ring beam

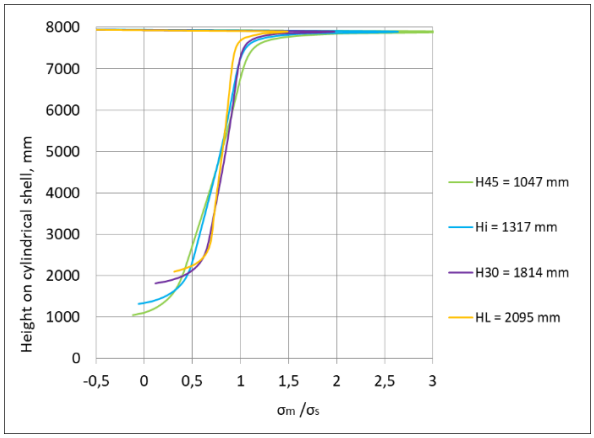

b) with openings in the ring beam

Fig. 11. Change of ratio $\sigma_{x,m}/\sigma_{x,s}$ by the height of the cylindrical shell 2 (D = 4 m, H = 8 m).

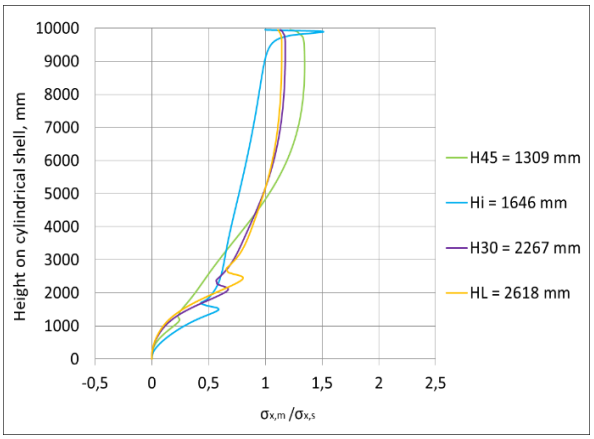

a) without openings in the ring beam

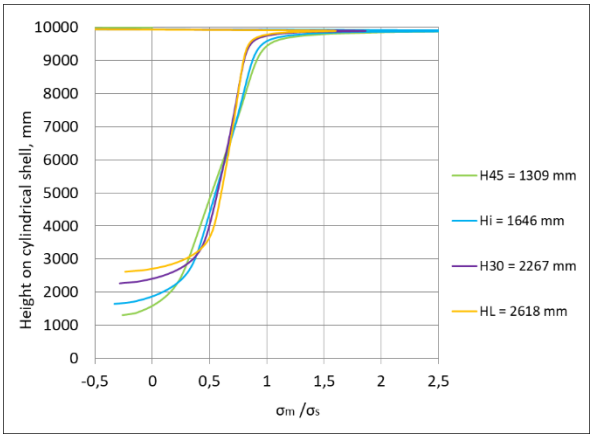

b) with openings in the ring beam

Fig. 12. Change of ratio $\sigma_{x,m}/\sigma_{x,s}$ by the height of the cylindrical shell 3 (D = 5 m, H = 10 m).

Obviously removing of material from the space between the supports, see Fig. 5 and 6, has its influence. At least the diagrams showing the changes of the ratio $\sigma_{x,m}/\sigma_{x,s}$ by the height of shell have different shape. More important is that the values of the stresses $\sigma_{x,m}$ and $\sigma_{x,s}$ in models with openings become equal on the bigger height. It means that the ways of transfer of compression stresses by the height are different for the continual bodies and for the bodies with openings.

Moreover, if on the models shown on Figs. 5(b) and 6 the base reactions obviously are redistributed on the height only through the work on compression of the cylindrical shell as an arch, this is not the same for the shell without openings. From where it can be concluded that the concept shown in EN 1993-4-1 has a grain rationality.

On the Figs. 10-12 we can see ratio $\sigma_{x,m}/\sigma_{x,s} > 1.0$. It means that in the part of the shell meridional stresses in the middle, between supports, are bigger than the stresses above the supports. The similar phenomena was observed in the previous research of Zdravkov (2017a) and (2017b).

The results of carried out Buckling Analysis, reporting buckling above the vertical stiffeners and stiffening ring above them, see Fig. 13(a), for every one shell are as follow:

a) shell 1 – diameter D = 3 m, height H = 6 m

Height of stiffeners	Buckling reserve capacity k	
	shell without openings	shell with openings
H_{45} = 785 mm	31.416	30.675
H_{I} = 987 mm	36.381	34.703
H_{30} = 1360mm	42.644	41.416
H_{L} = 1 571 mm	46.33	44.558

b) shell 2 – diameter D = 4 m, height H = 8 m

Height of stiffeners	Buckling reserve capacity k	
	shell without openings	shell with openings
H_{45} = 1047mm	24.943	23.468
H_{I} = 1317 mm	28.809	26.897
H_{30} = 1814mm	34.478	34.021
H_{L} = 2095mm	38.277	36.243

c) shell 3 – diameter D = 5 m, height H = 10m

Height of stiffeners	Buckling reserve capacity k	
	shell without openings	shell with openings
H_{45} = 1309mm	5.434	5.363
H_{I} = 1646 mm	6.463	6.306
H_{30} = 2267mm	7.951	7.671
H_{L} = 2618 mm	8.857	8.374

It gives impression that the reserve of the bearing capacity *k* in the tight shell is always bigger. Which is another proof that the redistributing of discrete base reactions on the height is not only achieved by compression forces as it is shown on Fig. 3.

It is important to notice that when the cylindrical shells without openings are researched, the first form of buckling is always caused by shearing. The area of buckling is in both sides of the vertical stiffeners, see Fig. 13(a).

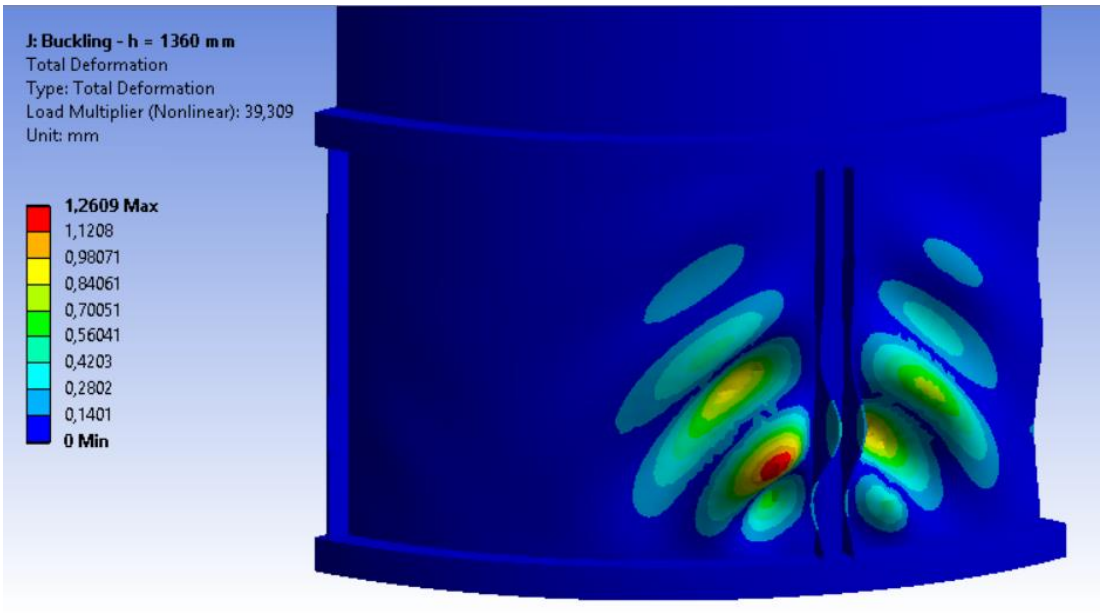

a) buckling due to shearing

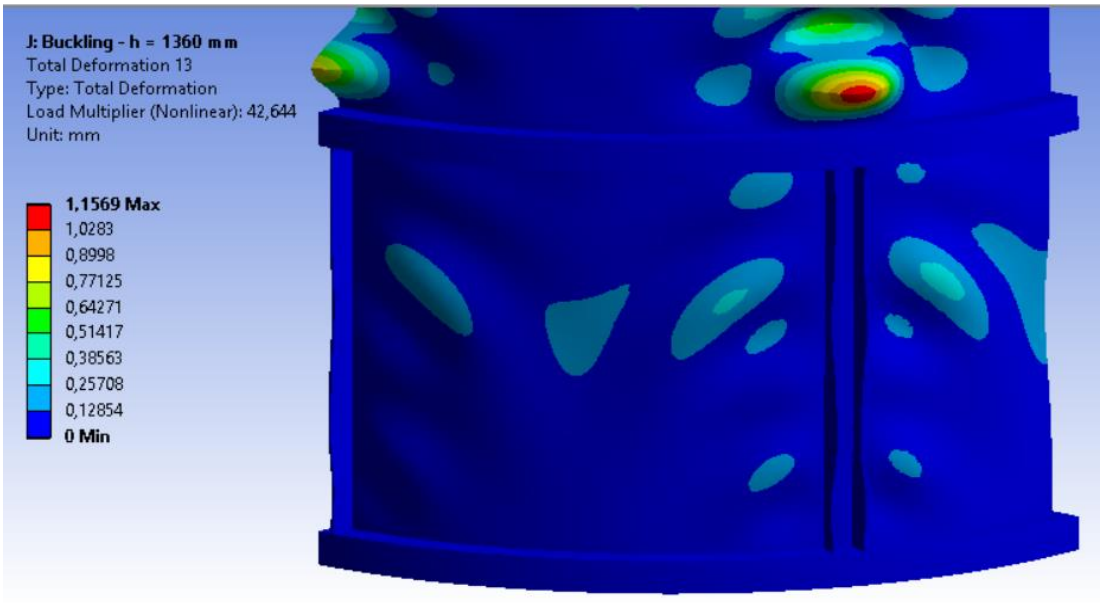

b) buckling due to compression

Fig. 13. Modes of buckling in the cylindrical shells.

4. Conclusions

The current research, made for six cylindrical shells on discrete supports, shows that the continual shells have different behaviour than the shells with openings between the supports.

From where could be concluded that the reactions of discrete supports are not distributed on the height only by work of the cylindrical shell on compression above them, as an arch. In the conception of EN 1993-4-1 for dividing the cylindrical body of the silo into discretely supported ring beam and cylindrical body there is some truth. For that reason the body of silo above the supports should be checked for:

- buckling in the area above vertical stiffeners, caused by meridional (axial) forces;
- buckling to left or right of vertical stiffeners, due to shearing forces.

REFERENCES

ANSYS 17 (2016). Ansys Inc., Canonsburg, PA, USA.

API Standard 650 (2013). Welded Tanks for Oil Storage, Twelfth Edition. American Petroleum institute.

Calladine CR (1983). Theory of Shell Structures. Cambridge University Press, Cambridge, U.K.

EN 10025-2 (2004). Hot rolled products of structural steels - Part 2: Technical delivery conditions for non-alloy structural steels. European Committee for Standardization, Brussels.

EN 1991-4 (2006). Eurocode 1 - Actions on structures - Part 4: Silos and tanks. European Committee for Standardization, Brussels.

EN 1993-1-6 (2007). Design of steel structures - Part 1-6: Strength and stability of shell structures. European Committee for Standardization, Brussels.

EN 1993-4-1 (2007). Design of steel structures - Part 4-1: Silos. European Committee for Standardization, Brussels.

Rotter JM (1985). Analysis and Design of Ringbeams. *In "Design of Steel Bins for Storage of Bulk Solids"*, J. M. Rotter, ed., University of Sydney, Sydney, Australia, 164 –183.

Topkaya C, Rotter JM (2011a). Ring beam stiffness criterion for column supported metal silos. *ASCE Journal of Engineering Mechanics*, 134, 846-853.

Topkaya C, Rotter JM (2011b). Stiffness of silo supporting ring beams resting on discrete supports. *6th International Conference on Thin-Walled Structures*, Timisoara, Romania.

Topkaya C, Rotter JM (2014). Ideal location of intermediate ring stiffeners on discretely supported cylindrical shells. *Journal of Engineering Mechanics*, 140(4), 04013001, 1-10.

Vlasov VZ (1961). Thin-Walled Elastic Beams. National Science Foundation, Washington, DC.

Vlasov VZ (1964). General theory of shells and its applications in engineering. *NASA Technical Translation*, TTF-99, Washington, DC.

Zdravkov LA (2017a). Vertical stiffeners and internal pressure - influencing factors on distribution of meridional stresses in steel silos on discrete supports. *Challenge Journal of Structural Mechanics,* 3(3), 123-128.

Zdravkov LA (2017b). Influence of intermediate rings and height of skirt on effective width of compression zone in junction column - cylindrical shell of steel silo. *International Jubilee Scientific Conference "75th Anniversary of UACEG"*, Sofia.

Zdravkov LA (2018). Influencing factors on effective width of compressed zone in joint column - cylindrical shell of steel silo. *Challenge Journal of Structural Mechanics,* 4(1), 1-8.

Zeybek Ö, Topkaya C, Rotter JM (2015). Strength and stiffness requirements for intermediate ring stiffeners on discretely cylindrical shells. *Thin-Walled Structures*, 96, 64-74.

Zeybek Ö, Topkaya C, Rotter JM (2017). Requirements for intermediate ring stiffeners placed below the ideal location on discretely supported shells. *Thin-Walled Structures*, 115, 21-33.

Zeybek Ö, Topkaya C, Rotter JM (2019). Analysis of silo supporting ring beams resting on discrete supports. *Thin-Walled Structures*, 135, 285-286.